Article

Mitochondrial transfer mediates endothelial cell engraftment through mitophagy

https://doi.org/10.1038/s41586-024-07340-0

Received: 10 April 2023

Accepted: 20 March 2024

Published online: 01 May 2024

Check for updates

Ruei-Zeng Lin[1,2], Gwang-Bum Im[1,2], Allen Chilun Luo[1], Yonglin Zhu[1,2], Xuechong Hong[1,2], Joseph Neumeyer[1], Hong-Wen Tang[3], Norbert Perrimon[3] & Juan M. Melero-Martin[1,2,4]✉

Ischaemic diseases such as critical limb ischaemia and myocardial infarction affect millions of people worldwide[1]. Transplanting endothelial cells (ECs) is a promising therapy in vascular medicine, but engrafting ECs typically necessitates co-transplanting perivascular supporting cells such as mesenchymal stromal cells (MSCs), which makes clinical implementation complicated[2,3]. The mechanisms that enable MSCs to facilitate EC engraftment remain elusive. Here we show that, under cellular stress, MSCs transfer mitochondria to ECs through tunnelling nanotubes, and that blocking this transfer impairs EC engraftment. We devised a strategy to artificially transplant mitochondria, transiently enhancing EC bioenergetics and enabling them to form functional vessels in ischaemic tissues without the support of MSCs. Notably, exogenous mitochondria did not integrate into the endogenous EC mitochondrial pool, but triggered mitophagy after internalization. Transplanted mitochondria co-localized with autophagosomes, and ablation of the PINK1–Parkin pathway negated the enhanced engraftment ability of ECs. Our findings reveal a mechanism that underlies the effects of mitochondrial transfer between mesenchymal and endothelial cells, and offer potential for a new approach for vascular cell therapy.

Ischaemic diseases, including critical limb ischaemia and myocardial infarction, affect millions annually, and necessitate surgical interventions such as vascular grafts to revascularize tissues distal to blockages[1]. However, inadequate revascularization persists, owing to challenges in regenerating microvascular beds in ischaemic areas[4]. Although the delivery of angiogenic growth factors to stimulate local angiogenesis has been investigated[5], this approach is limited by the disrupted tissue microenvironment in ischaemic regions[6]. Consequently, EC transplantation remains a priority in vascular medicine.

A key challenge for EC therapies is the requirement for a secondary cell type to support engraftment. Although ECs can self-assemble into vascular structures, co-transplantation with perivascular cells is essential for robust engraftment and functional blood vessel formation in vivo[2]. Sources of perivascular cells include smooth muscle cells, pericytes, fibroblasts and MSCs[7]. However, the use of multiple cell types complicates clinical translation and increases the complexity of phase I studies, and thus there is a reluctance to use two or more different cell types in clinical trials.

The mechanisms by which perivascular cells facilitate EC engraftment are not fully understood. Here we show that MSCs transfer mitochondria to ECs through tunnelling nanotubes (TNTs) during transplantation, and that this process is crucial for successful EC engraftment in vivo. This observation aligns with previous findings of the transfer of mitochondria from MSCs to other cells, such as lung alveolar epithelial cells and neurons, during tissue repair[8,9]. Building on this insight, we devised a novel strategy: pre-emptively transplanting exogenous mitochondria into ECs to enhance engraftment in vivo. This approach induced a transient cytoprotective effect through mitophagy, enabling the engraftment of ECs without the support of MSCs. Our findings suggest a potential for a single-cell therapy strategy based on autologous EC engraftment, which might facilitate clinical translation.

EC engraftment requires stromal cells

To investigate engraftment, we used a xenograft model in which human ECs were combined with or without supporting MSCs in a collagen-based hydrogel, and the mixture was subcutaneously implanted into immunodeficient nude mice (Extended Data Fig. 1). Implants containing only ECs did not produce perfused grafts by day 7, and there was a rapid loss of EC viability within the first 72 h after transplantation. By contrast, co-implanting ECs with MSCs significantly improved EC viability and generated an extensive network of microvessels connected to the host circulatory system (Extended Data Fig. 1a–d). The marked difference in microvessel density owing to the presence of MSCs was evident in histological analysis (Extended Data Fig. 1a,b). Engraftment disparity was confirmed using bioluminescence imaging of luciferase-expressing ECs (lucif-ECs) for up to four weeks (Extended Data Fig. 1c,d). MSC dependency for engraftment and functional blood vessel formation in vivo was further substantiated with various types of primary human ECs, including human umbilical vein endothelial (HUVECs) cells, endothelial colony-forming cells

[1]Department of Cardiac Surgery, Boston Children's Hospital, Boston, MA, USA. [2]Department of Surgery, Harvard Medical School, Boston, MA, USA. [3]Department of Genetics, Howard Hughes Medical Institute, Harvard Medical School, Boston, MA, USA. [4]Harvard Stem Cell Institute, Cambridge, MA, USA. ✉e-mail: juan.meleromartin@childrens.harvard.edu

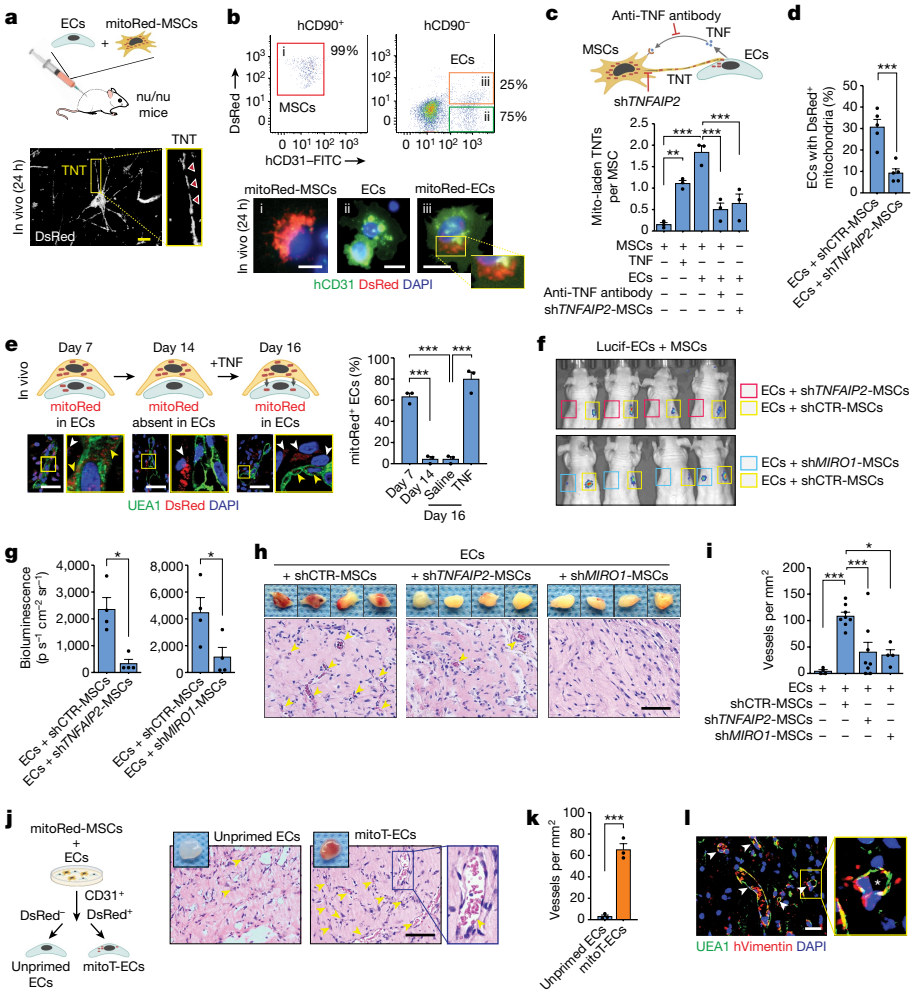

Fig. 1 | MSCs facilitate EC engraftment through mitochondrial transfer. **a**, Illustration of mitoRed-MSCs with ECs in mice, showing TNTs with DsRed$^+$ mitochondria at 24 h. **b**, hCD90$^-$hCD31$^+$ ECs with DsRed$^+$ mitochondria (mitoRed-ECs) identified by flow cytometry and immunofluorescence; CD90 identifies MSCs. **c**, Quantification of TNTs containing DsRed$^+$ mitochondria in MSC–EC co-cultures. The effects of anti-TNF antibody treatment or *TNFAIP2* silencing are shown ($n = 3$; one-way ANOVA with Bonferroni's post-test). **d**, Quantification of ECs receiving DsRed$^+$ mitochondria from sh*TNFAIP2*-MSCs or control shCTR-MSCs ($n = 5$; unpaired two-tailed *t*-test). **e**, Temporal analysis of DsRed$^+$ mitochondria in ECs after engraftment. UEA1$^+$ ECs show mitoRed at day 7, and this is absent by day 14. TNF triggers the reactivation of mitoRed transfer ($n = 3$; one-way ANOVA with Bonferroni's post-test). **f**,**g**, Bioluminescence of lucif-EC and MSC grafts at day 7. **f**, The effects of *TNFAIP2* and *MIRO1* silencing on EC engraftment were assessed. **g**, Quantification at day 7 ($n = 4$; paired two-tailed *t*-test). **h**, H&E-stained grafts at day 7, revealing blood vessels (arrowheads) after *TNFAIP2* and *MIRO1* silencing. **i**, Microvessel perfusion density at day 7 ($n = 4$–8; one-way ANOVA with Bonferroni's post-test). **j**, Schematic of twenty-four-hour co-culture of ECs and mitoRed-MSCs; CD31$^+$DsRed$^+$ mitoT-ECs were FACS sorted. H&E staining of grafts implanted in mice shows day-7 perfused vessels (arrowheads). **k**, Perfused microvessel density at day 7 ($n = 3$; unpaired two-tailed *t*-test). **l**, Grafts (mitoT-ECs) at day 7, immunostained for human-specific vessels (UEA1$^+$hVimentin$^+$; arrowheads, asterisk). Data are mean ± s.e.m.; *n* are biological replicates (**c**,**d**) and independent animals (**e**,**g**,**i**,**k**); $^*P \le 0.05$, $^{**}P \le 0.01$, $^{***}P \le 0.001$. Scale bars, 10 µm (**a**,**b**); 50 µm (**e**,**l**); 100 µm (**h**,**j**). Related results in Extended Data Figs. 1–4.

(ECFCs) and white-adipose-tissue-derived ECs (wat-ECs) (Extended Data Fig. 1a,b).

Perivascular cells have a crucial role in modulating blood vessel stability and function[10]. However, the mechanisms by which perivascular cells facilitate EC engraftment remain partially understood. MSCs secrete a range of angiogenic factors that are absent in ECs (Extended Data Fig. 1f). Nonetheless, supplementing with MSC-secreted factors could not replace MSCs and was insufficient to support early survival (24 h after implantation; Extended Data Fig. 1e) or the blood-vessel-forming ability of ECs at day 7 (Extended Data Fig. 1g), indicating that the supportive role of MSCs is not exclusively paracrine. Moreover, inhibiting PDGFR signalling (using tyrphostin AG1296), which delays MSC–EC juxtaposition[11], did not affect EC engraftment (Extended Data Fig. 1e,g,h), suggesting that the PDGFR-signalling-mediated perivascular contact is not essential for maintaining EC viability under immediate post-implantation stress.

Mitochondrial transfer from MSCs to ECs via TNTs

Previous studies have shown that MSCs can naturally transfer mitochondria to other parenchymal cells, including lung alveolar epithelial cells and neurons, during regenerative processes[8,9]. This phenomenon was found to be crucial for cell survival. However, mitochondrial transfer in the vascular system has not been described. We investigated whether mitochondrial transfer from MSCs could mediate EC survival during engraftment. MSCs were transfected with a piggyBac transposon containing a mito-tag, rendering all mitochondria DsRed$^+$ (referred to as mitoRed-MSCs). Histological examination of 24-h grafts revealed ultrafine and long protrusions extending from MSCs containing DsRed$^+$ mitochondria (Fig. 1a). These structures were also observed in vitro when mitoRed-MSCs were co-cultured with ECs (Extended Data Fig. 2a), and resembled TNTs, which have been previously implicated in mitochondrial transfer. These protrusions had aligned DsRed$^+$

mitochondria, F-actin and microtubules (Extended Data Fig. 2a,b), consistent with TNTs[12]. Flow cytometric and immunofluorescence analyses of grafts seeded with ECs and mitoRed-MSCs revealed that, after 24 h in vivo, around 25% of ECs (human (h)CD90$^-$hCD31$^+$ cells) contained DsRed$^+$ mitochondria, suggesting mitochondrial transfer from mitoRed-MSCs (Fig. 1b and Extended Data Fig. 2c,d). Notably, mitochondrial transfer required direct MSC–EC communication, was affected by cell proportions and increased significantly under hypoxic (1% oxygen) stress (Extended Data Fig. 2e,f). TNT formation was largely unidirectional, with minimal mitochondrial transfer from ECs to MSCs (Extended Data Fig. 2g–i).

We examined the role of TNF, a potent inducer of TNT formation[13] that is upregulated after the activation of ECs in three-dimensional (3D) cultures (Extended Data Fig. 3a,b). Blocking TNF with a monoclonal antibody significantly reduced the presence of mitochondria-containing TNTs in our co-culture model (Fig. 1c). Furthermore, transcriptional abrogation of TNFAIP2, a regulator of TNT formation[14], in mitoRed-MSCs (using short hairpin RNA; shRNA) diminished the appearance of TNTs (Fig. 1c and Extended Data Fig. 3d,e). Inhibiting the formation of TNTs by silencing *TNFAIP2* significantly blocked mitochondrial transfer (Fig. 1d), reinforcing the idea that mitochondrial transfer from MSCs to ECs occurs through TNTs.

In vivo, mitochondrial transfer was transient. Transfer began immediately after cell transplantation (24 h; Fig. 1b) and persisted during blood vessel formation, with DsRed$^+$ mitochondria observed in ECs lining newly formed blood vessels on day 7 (Fig. 1e and Extended Data Fig. 4). By day 14, once the vasculature stabilized, DsRed$^+$ mitochondria were restricted to perivascular MSCs and largely absent in ECs (Fig. 1e), indicating that mitochondrial transfer had ceased. Notably, local administration of TNF on day 14 reactivated mitochondrial transfer from MSCs, resulting in the presence of DsRed$^+$ mitochondria in ECs (Fig. 1e and Extended Data Fig. 4). These data suggest that there is a dynamic relationship between mitochondrial transfer and the vasculature's physiological state (stressed and activated versus stable). Specifically, mitochondria appear to be continuously transferred between MSCs and ECs during the early post-transplantation period, a phenomenon driven by environmental stress, including increased local levels of TNF. This continuous transfer is active in the early days following transplantation, facilitating the integration of mitochondria into ECs. However, as MSCs and ECs organize into perfused vessels, the cellular environment stabilizes, causing cells to enter a quiescent state. This stabilization halts the natural transfer of mitochondria.

Mitochondrial transfer enables EC engraftment

The effect of mitochondrial transfer on EC engraftment was substantial. Transcriptional abrogation of TNT formation (through shRNA silencing of *TNFAIP2*; Extended Data Fig. 3d,e) or mitochondrial mobilization in TNTs (by silencing the expression of mitochondrial Rho GTPase 1 (*MIRO1*; also known as *RHOT1*); Extended Data Fig. 3f–i) in MSCs significantly impaired EC engraftment (Fig. 1f,g). ECs exhibited a reduced ability to form perfused microvessels by day 7 when implanted with either sh*TNFAIP2*-MSCs or sh*MIRO1*-MSCs, compared with control MSCs (Fig. 1h,i). Thus, the formation of TNTs and the subsequent transfer of mitochondria from MSCs are essential for robust EC engraftment.

We investigated whether MSCs could pre-emptively transfer mitochondria to ECs before transplantation. ECs that were sorted as CD31$^+$DsRed$^+$ cells from a 24-h co-culture with mitoRed-MSCs (referred to as mitoT-ECs) exhibited a significantly enhanced engraftment ability. Grafts that contained only mitoT-ECs exhibited extensive networks of perfused human microvessels surrounded by mouse perivascular cells (Fig. 1j–l). Conversely, grafts with ECs that did not receive transferred DsRed$^+$ mitochondria from MSCs (unprimed ECs) did not vascularize (Fig. 1j–l). Our findings suggest that co-culturing with MSCs allowed a subset of ECs to receive mitochondria through TNTs, conferring enhanced biological properties. Specifically, these primed mitoT-ECs showed an improved capacity to engraft and form functional blood vessels in vivo without direct MSC support.

Artificial mitochondrial transplantation into ECs

Inspired by the natural transfer of mitochondria from MSCs (Fig. 1), we investigated whether artificially transplanting exogenous mitochondria into ECs could enhance engraftment. Mitochondria were isolated from MSCs and incubated with EC cultures, in which uptake occurred in around 4 h (Fig. 2a and Extended Data Fig. 5a–c; ECs that artificially received mitochondria are referred to as mitoAT-ECs). The number of mitochondria used for artificial transplantation corresponded to a 3:1 ratio (that is, mitochondria from three donor MSCs for each recipient EC). Flow cytometry analysis revealed that the percentage of mitoAT-ECs that effectively received exogenous mitochondria was exceptionally high (around 90%; Extended Data Fig. 5b). This process of mitochondrial incorporation into cells by simple co-incubation is regulated through micropinocytosis (a clathrin-independent form of endocytosis)[15]. Internalization of exogenous mitochondria was confirmed with confocal microscopy, using mitoRed-MSCs as donor cells and tracing the DsRed$^+$ signal at appropriate focal planes (Extended Data Fig. 5c). Transmission electron microscopy (TEM) further confirmed the internalization of mitochondria isolated from mitoAPEX2-MSCs and the presence of APEX2-labelled mitochondria in ECs (Extended Data Fig. 5d–h).

Artificial mitochondrial transplantation into ECs mimicked the effects of natural mitochondrial transfer from MSCs through TNTs, resulting in transient cytoprotective attributes, such as enhanced metabolic activities (Fig. 2b–d and Extended Data Fig. 6a–c), resistance to apoptosis (Fig. 2f and Extended Data Fig. 6d,e) and increased cellular mobility (Fig. 2e and Extended Data Fig. 6f,g). Of note, transplantation of other organelles (namely, lysosomes) did not produce these functional enhancements in ECs (Extended Data Fig. 6i,j). Transplanting mitochondria from eight different types of donor cell, including primary cells from various species and immortalized cell lines, produced similar effects on mitoAT-ECs (Extended Data Fig. 6g), suggesting that the origin of the exogenous mitochondria is not critical.

MitoAT-EC engraftment significantly improved after mitochondrial transplantation, without the need for MSCs (Fig. 2g,h). Subcutaneous grafts seeded with only mitoAT-ECs that had received exogenous mitochondria 4 h before implantation contained extensive networks of perfused human microvessels by day 7 (Fig. 2i–k), whereas control EC grafts failed to vascularize. The density of microvessels in grafts with mitoAT-ECs alone was comparable to that of grafts containing ECs with MSCs (Fig. 2j), indicating that exogenous mitochondrial transplantation can compensate for the absence of supporting MSCs during engraftment.

MitoAT-EC engraftment was also effective in ischaemic tissues. MitoAT-ECs showed a significantly higher level of engraftment into ischaemic hindlimbs (femoral ligation) in diabetic nude mice than did control ECs (Fig. 2l), resulting in a robust presence of human vessels in the ischaemic muscle by day 7 (Fig. 2m). This enhanced engraftment translated into improved blood flow in the affected limbs for up to three weeks (Fig. 2n,o) and prevented the development of necrotic tissue in mice that received mitoAT-ECs (Fig. 2p). Our findings show that artificial transplantation of exogenous mitochondria can enhance the intrinsic ability of human ECs to engraft and revascularize ischaemic tissues without additional supporting cells.

Exogenous mitochondria are depolarized

Receiving exogenous mitochondria by natural cell-to-cell transfer (Fig. 1) or artificial transplantation (Fig. 2) improved the fitness of ECs, suggesting that transplanted mitochondria must have remained

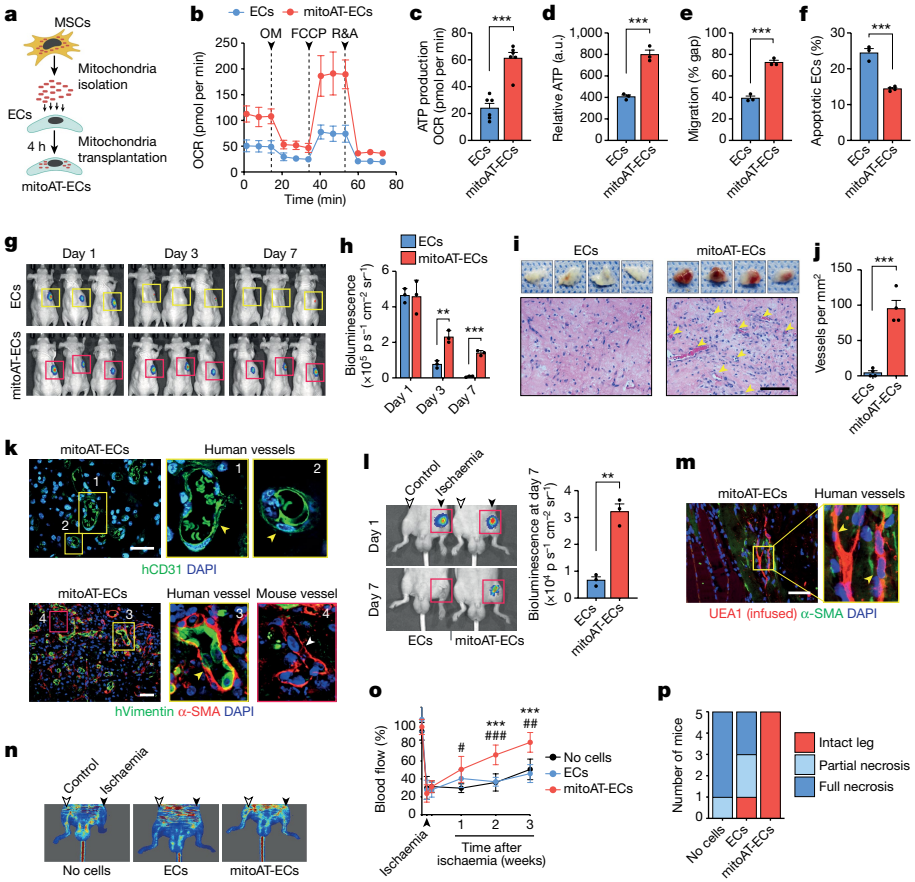

Fig. 2 | Exogenous mitochondrial transplantation enhances EC engraftment. **a**, Diagram of the mitochondrial isolation and transplantation process. **b**, Seahorse analysis shows enhanced respiration in mitoAT-ECs 24 h after transplantation ($n = 6$). OCR, oxygen consumption rate; OM, oligomycin; FCCP, carbonyl cyanide-*p*-trifluoromethoxyphenyl hydrazone; R&A, rotenone and antimycin A. **c**, ATP production from Seahorse analysis. $^{***}P \leq 0.001$ ($n = 6$; unpaired two-tailed *t*-test). **d**–**f**, Functional comparison of ECs and mitoAT-ECs: ATP production (**d**), migration capacity (**e**) and apoptosis after H_2O_2 exposure (**f**). a.u., arbitrary units. $^{***}P \leq 0.001$ ($n = 3$; unpaired two-tailed *t*-test). **g**, Bioluminescence imaging of grafts with ECs or mitoAT-ECs. **h**, Quantification at days 1, 3 and 7. $^{**}P \leq 0.01$, $^{***}P \leq 0.001$ ($n = 3$; unpaired two-tailed *t*-test). **i**–**k**, Grafts with ECs or mitoAT-ECs implanted in mice. **i**, Macroscopic view at day 7. H&E staining shows perfused vessels (arrowheads) in mitoAT-EC grafts. **j**, Microvessel density at day 7. $^{***}P \leq 0.001$ ($n = 3$; unpaired two-tailed *t*-test). **k**, Immunofluorescent staining of human-specific vessels at day 7 in mitoAT-EC grafts. **l**–**p**, Hindlimb ischaemia in mice injected with luciferase-labelled ECs or mitoAT-ECs. **l**, Bioluminescence images on days 1 and 7. $^{**}P \leq 0.01$ ($n = 3$; unpaired two-tailed *t*-test). **m**, Immunofluorescence of human vessels in ischaemic muscle with mitoAT-ECs (day 7). **n**, Laser Doppler images of ischaemic hindlimbs at three weeks. **o**, Blood flow quantified by laser Doppler. $^{***}P \leq 0.001$, compared to ECs. $^{\#}P \leq 0.05$, $^{\#\#}P \leq 0.01$, $^{\#\#\#}P \leq 0.001$, compared to no cells ($n = 5$; one-way ANOVA with Bonferroni's post-test analysis). **p**, Mice with necrosis or intact legs in each group at three weeks ($n = 5$). Data are mean ± s.e.m.; *n* indicates biological replicates (**b**–**f**) and independent animals (**h**,**j**,**l**,**o**,**p**). Scale bars, 100 μm (**i**); 40 μm (**k**); 50 μm (**m**). Related results in Extended Data Figs. 5 and 6.

functional and must have been incorporated into the recipient cells' endogenous mitochondrial pool. However, exogenous mitochondria did not maintain their functional competence during isolation from MSCs and incubation with ECs. After exposure to EGM2 culture medium containing a high concentration of Ca^{2+} (around 1.6 mM), mitochondria were immediately and irreversibly compromised, with depolarization of their membrane potential owing to a rapid overload of Ca^{2+} mediated by the mitochondrial Ca^{2+} uniporter (Fig. 3a,b). Despite this, the artificial transplantation of depolarized exogenous mitochondria consistently enhanced EC fitness (Fig. 2), which was puzzling.

We investigated whether transplanted mitochondria integrate and persist in recipient ECs using a mitochondrial DNA (mtDNA) genotyping approach that detects heteroplasmy. After sequencing mtDNA in ECs and MSCs from two separate individuals, we identified four loci at the hypervariable regions (HVR1 and HVR2) with single-nucleotide differences (Extended Data Fig. 7). After artificial mitochondrial transplantation, we estimated the percentage of donor (MSCs) versus endogenous (ECs) mtDNA in recipient mitoAT-ECs by measuring heteroplasmy in the selected loci. This analysis revealed that 24 h after transplantation, around 12% of the total mtDNA in mitoAT-ECs corresponded to exogenous mitochondria, but by day 7, donor mtDNA was undetectable, indicating that the transplanted mitochondria persisted for only a limited time in recipient mitoAT-ECs (Fig. 3c).

To determine whether transplanted mitochondria fuse with the recipient mitochondrial pool, we used a split-GFP system. We genetically split GFP into two components (GFP-1–10 and GFP-11; only when these two components are together can GFP emit its fluorescent signal) and added a mito-tag (mt) to send them to the mitochondrial matrix (Extended Data Fig. 8). We then transduced donor mitoRed-MSCs with mtGFP-11 and recipient ECs with mtGFP-1–10 and investigated mitochondrial fusion after both natural transfer (co-culture) and artificial transplantation. Direct co-culture with mitoRed-MSCs(mtGFP-11) resulted in minimal fusion of transferred mitochondria with the endogenous mitochondrial pool in ECs. Transferred $DsRed^+$ mitochondria comprised around 13.3% of the total mitochondrial content in recipient ECs by 24 h, but only around 1.7% effectively fused (that is, $DsRed^+GFP^+$) (Extended Data Fig. 8c). However, with artificially transplanted mitochondria (around 8.2% of all mitochondria at 4 h), the GFP signal was virtually undetectable in mitoAT-ECs (Fig. 3d and Extended Data Fig. 8d), suggesting negligible mitochondrial fusion.

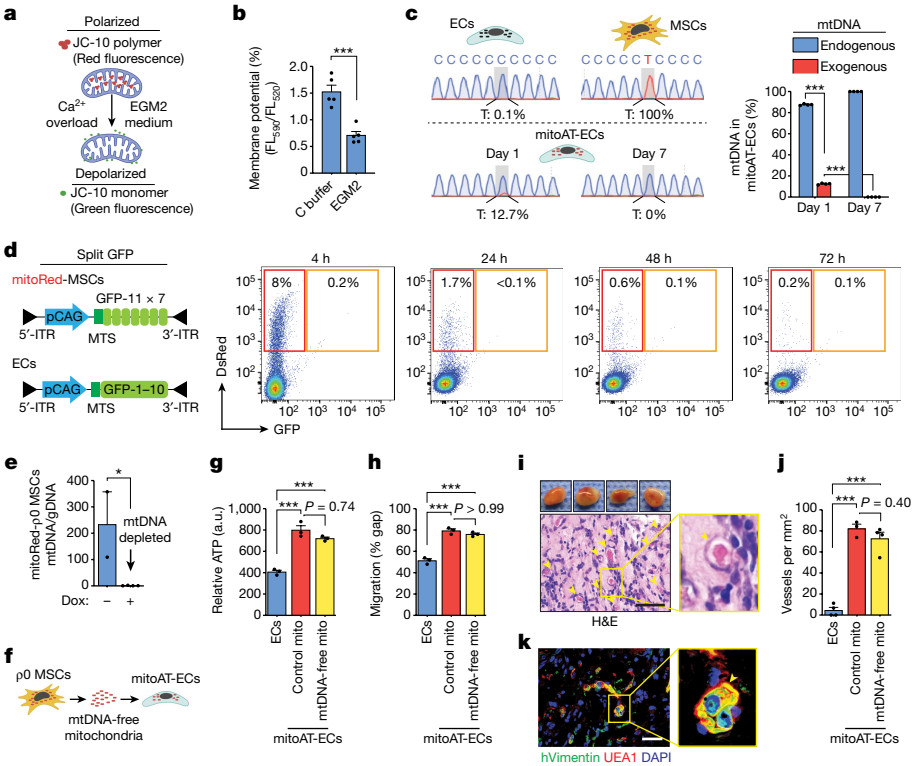

Fig. 3 | Transplanted mitochondria are not incorporated into the recipient pool. a, Schematic of JC-10 assay for measuring mitochondrial depolarization. **b**, Changes in mitochondrial membrane potential (FL_{590}/FL_{520} ratio) in MSC-derived mitochondria in Ca^{2+}-free (C buffer) and Ca^{2+}-containing (EGM2) medium ($n = 5$; unpaired two-tailed t-test). **c**, Heteroplasmy in mtDNA of ECs and MSCs. Left, mtDNA sequencing at a distinct locus showing a single-nucleotide difference between ECs and MSCs. Right, exogenous versus endogenous mtDNA in mitoAT-ECs was assessed by sequencing heteroplasmic sites at days 1 and 7 after transplantation ($n = 4$ loci; unpaired two-tailed t-test). **d**, Left, schematic of the split-GFP system with GFP-1–10 and GFP-11 in the mitochondrial matrix of ECs and mitoRed-MSCs, respectively. ITR, inverted terminal repeats of piggyBac transposon. Right, flow cytometry of mitoAT-EC mitochondria to detect fused $DsRed^+GFP^+$ mitochondria over time (time points are hours after mitochondria transplantation). **e**, mtDNA-free MSCs (mitoRed-ρ0-MSCs) with Dox-inducible MTS-EcoRI-GFP for mtDNA degradation, assessed by qPCR for mtDNA normalized to genomic DNA (gDNA) with or without Dox ($n = 4$; unpaired two-tailed t-test). **f**, Schematic of transplantation of mtDNA-free mitochondria into ECs. **g**,**h**, Comparison of ECs and mitoAT-ECs: ATP production (**g**) and migration (**h**) ($n = 3$; unpaired two-tailed t-test). **i**, Grafts of mtDNA-free mitoAT-ECs in mice. Macroscopic view at day 7. H&E staining reveals perfused vessels (arrowheads). **j**, Perfused microvessel density at day 7 ($n = 3$; unpaired two-tailed t-test). **k**, Human-specific ($hVimentin^+UEA1^+$) vessel immunofluorescence at day 7 (arrowheads). Data are mean ± s.e.m.; n indicates biological replicates (**b**,**e**,**g**,**h**) and independent animals (**j**); $^*P \le 0.05$, $^{***}P \le 0.001$. Scale bars, 100 µm (**i**); 50 µm (**k**). Related results in Extended Data Figs. 7–9.

mtDNA-free mitochondria enhance EC function

To further confirm that donor mitochondria do not need to be functional, we generated mitoRed-MSCs without mtDNA (called mitoRed-ρ0-MSCs). These mitoRed-ρ0-MSCs contained a doxycycline (Dox)-inducible gene encoding an EcoRI restriction endonuclease fused to a mitochondrial targeting sequence (MTS) and a GFP reporter (Extended Data Fig. 9a). After administering Dox for 48 h, the MTS-EcoRI-GFP complex co-localized with $DsRed^+$ mitochondria, completely degrading the endogenous mtDNA in mitoRed-ρ0-MSCs (Fig. 3e and Extended Data Fig. 9b). Although dysfunctional, mitoRed-ρ0-MSCs were viable. Transferring mtDNA-free mitochondria from mitoRed-ρ0-MSCs (Fig. 3f) had similar effects on ECs to those that were observed with normal functional mitochondria, including increased ATP (Fig. 3g and Extended Data Fig. 9c,d), migratory activity (Fig. 3h) and in vivo engraftment ability (Fig. 3i–k). These results indicate that donor mitochondria do not need to be functional to enhance the fitness of ECs, implying an alternative role as a trigger.

Transplanted mitochondria trigger mitophagy

To gain insights into the transcriptional changes produced in ECs by incorporating exogenous mitochondria through either co-culture with MSCs (mitoT-ECs) or artificial transplantation (mitoAT-ECs), we performed RNA sequencing (RNA-seq) analysis (Fig. 4a–d). ECs that were co-cultured with MSCs but did not receive exogenous mitochondria (unprimed ECs) served as controls. Globally, there were hundreds of differentially expressed genes across all EC groups (Fig. 4a). Hierarchical clustering analysis of differentially expressed genes revealed transcriptional proximity between samples from each EC group, and these associations were confirmed by principal component analysis (PCA) (Fig. 4b). To gain more insight into the transcriptional differences, we performed Gene Intology (GO) enrichment analysis. Notably, both mitoT-ECs and mitoAT-ECs exhibited significant enrichment in genes associated with mitochondrial respiration, ATP synthesis, the electron transport chain and oxidative phosphorylation, compared with unprimed ECs (Fig. 4c,d), consistent with their enhanced metabolic activities (Fig. 2b–d and Extended Data Fig. 6). Furthermore, quantitative PCR (qPCR) analysis of gene expression in mitoAT-ECs revealed a significant upregulation of several genes associated with mitochondrial biogenesis (Fig. 4e). Indeed, 24 h after mitochondrial transplantation, mitoAT-ECs had significantly more mitochondria (around twofold; normalized to nuclear protein content), compared with control ECs (Fig. 4f). In addition, western blot analyses confirmed that the mitochondrial content (TOM20 normalized to β-actin) was significantly higher in mitoAT-ECs than in control ECs, and that this

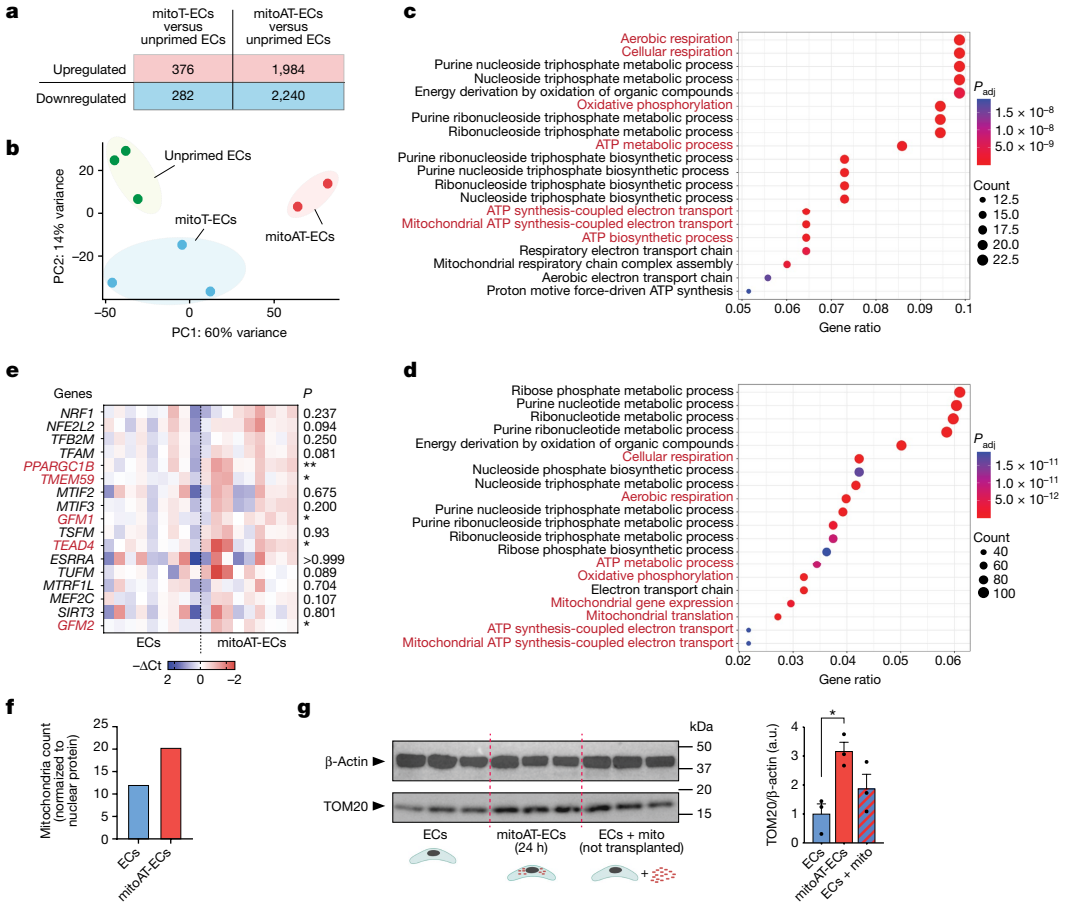

Fig. 4 | Insights into the enhancement of mitochondrial respiration and biogenesis in mitoT-ECs and mitoAT-ECs. a–**d**, Bulk RNA-seq of EC samples: (i) ECs with transplanted exogenous mitochondria (mitoAT-ECs); (ii) ECs gaining exogenous mitochondria through MSC co-culture (mitoT-ECs); and (iii) ECs in MSC co-culture without exogenous mitochondria uptake (unprimed ECs). **a**, Summary of differential gene expression. **b**, PCA. **c**,**d**, GO analysis (positive enrichment) for mitoT-ECs versus unprimed ECs (**c**) and for mitoAT-ECs versus unprimed ECs (**d**). Adjusted *P* values using Benjamini–Hochberg. **e**–**g**, Mitochondrial biogenesis after mitochondrial transplantation in mitoAT-ECs. **e**, Heat map of mRNA expression (qPCR) of mitochondrial biogenesis genes in mitoAT-ECs versus ECs. $^{*}P \leq 0.05$, $^{**}P \leq 0.01$ ($n = 9$ ECs and $n = 9$ mitoAT-ECs; unpaired two-tailed *t*-test). **f**, Mitochondrial content in mitoAT-ECs 24 h after transplantation, quantified by flow cytometry and normalized to nuclear protein, with pre-transplant ECs as control. **g**, Western blot evaluation of TOM20 for mitochondrial content in mitoAT-ECs. β-Actin was used as a housekeeping protein. Lysates from regular ECs and a mixture of ECs and exogenous mitochondria pre-transplantation (ECs + mito; not transplanted) served as controls. $^{*}P \leq 0.05$ ($n = 3$; one-way ANOVA with Bonferroni's post-test; mean ± s.e.m.). *n* are biological replicates (**a**–**e**,**g**). For gel source data, see Supplementary Fig. 1.

increase was higher than would result merely from the presence of exogenous mitochondria (Fig. 4g).

Our results did not support the idea that transplanted mitochondria were functionally incorporated into recipient ECs. Instead, 6–12 h after artificial transplantation, exogenous mitochondria co-localized with autophagosomes (Fig. 5a), and ULK1-mediated autophagic activity significantly increased in mitoAT-ECs (Fig. 5b and Extended Data Fig. 10). Most exogenous DsRed^{+} mitochondria (including those using mtDNA-free mitochondria from mitoRed-ρ0-MSCs) localized in LC3B^{+} autophagosomes (Fig. 5c).

Mitophagy refers to the selective autophagic degradation of mitochondria. To further investigate whether transplanting mitochondria triggered mitophagy in mitoAT-ECs, we targeted PTEN-induced putative protein kinase 1 (PINK1) and the E3 ubiquitin ligase Parkin, both well-established mediators of mitophagy[16]. During mitophagy, PINK1 accumulates on the outer mitochondrial membrane (OMM) of depolarized mitochondria and recruits Parkin from the cytosol. Parkin initiates the ubiquitination of numerous OMM proteins, leading to phagophore recruitment and autophagosome assembly[17]. Several lines of evidence suggest that the PINK1–Parkin pathway is involved in mitochondrial transplantation. First, we detected the presence of PINK1 in the isolated mitochondria by both flow cytometry and western blot analyses (Extended Data Fig. 10b,c). Also, immunofluorescence analysis of mitoAT-ECs revealed that approximately 23% of the DsRed-labelled exogenous mitochondria co-localized with cytoplasmic Parkin 24 h after transplantation (Extended Data Fig. 10d). Moreover, genetic ablation of *PINK1* (using shRNA) in donor mitochondria prevented autophagosome formation in mitoAT-ECs (Fig. 5d and Extended Data Fig. 10i). However, silencing *PINK1* in recipient ECs did not affect LC3B assembly, indicating that only internalized exogenous mitochondria trigger mitophagy. Similarly, silencing Parkin (encoded by *PRKN*) in recipient ECs abrogated the formation of LC3B^{+} autophagosomes in mitoAT-ECs, whereas silencing Parkin in mitochondrial donor MSCs had no effect (Fig. 5d and Extended Data Fig. 10i).

Collectively, these findings are consistent with the notion of the activation of mitophagy after the internalization of exogenous mitochondria, which, in turn, enhances mitochondrial biogenesis and results in mitoAT-ECs exhibiting improved respiration and cellular functions.

Mitophagy mediates EC engraftment

We next examined whether mitophagy regulated the engraftment of mitoAT-ECs. To do this, we first inhibited mitophagy in mitoAT-ECs by either silencing Parkin in the recipient ECs (sh*PRKN*-ECs) or PINK1 in the

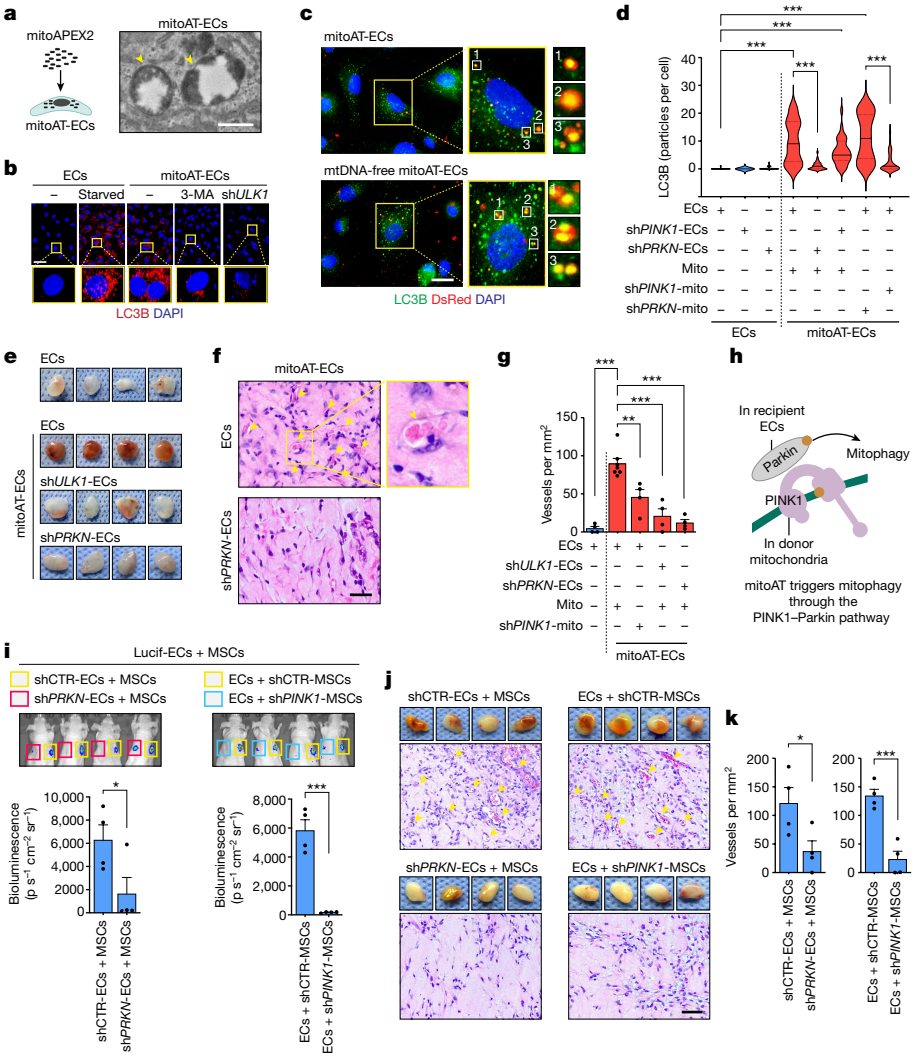

Fig. 5 | Enhanced engraftment ability in ECs mediated by mitophagy. **a**, Mitochondria isolated from mitoAPEX2-MSCs transplanted into ECs. TEM micrograph shows internalized APEX2$^+$ mitochondria co-localizing with autophagosomes in mitoAT-ECs after 24 h. **b**, Immunofluorescent staining of LC3B$^+$ autophagosomes in ECs and mitoAT-ECs. Starvation and mitochondrial transplantation increased LC3B$^+$ autophagosomes in ECs. Inhibiting autophagy with 3-methyladenine (3-MA) or silencing *ULK1* (sh*ULK1*) prevented LC3B+ autophagosome accumulation in mitoAT-ECs. **c**, Co-localization of exogenous DsRed$^+$ mitochondria and LC3B$^+$ autophagosomes in mitoAT-ECs. **d**, Effects of shRNA-mediated silencing of *PINK1* or *PRKN* (encoding Parkin) on LC3B$^+$ autophagosomes in mitoAT-ECs ($n = 30$ cells per group; one-way ANOVA with Bonferroni's post-test). **e**–**g**, Effects of shRNA-mediated silencing of *ULK1*, *PINK1* or *PRKN* on the engraftment ability of mitoAT-ECs. **e**, Macroscopic view of grafts at day 7. **f**, H&E-stained mitoAT-EC grafts show perfused vessels (arrowheads) at day 7. **g**, Microvessel density at day 7 ($n = 4$; $n = 8$ in ECs + mito; one-way ANOVA with Bonferroni's post-test). **h**, Schematic showing the roles of Parkin (recipient ECs) and PINK1 (donor mitochondria) in mitophagy activation in mitoAT-ECs. **i**–**k**, Effects of silencing *PINK1* and *PRKN* on the engraftment ability of ECs co-implanted with MSCs. **i**, Bioluminescence of grafts with lucif-ECs and MSCs at day 7. *PRKN* silenced in ECs (left) and *PINK1* silenced in MSCs (right). Quantification at day 7 ($n = 4$; paired two-tailed *t*-test). **j**, Macroscopic views and H&E staining of grafts with perfused vessels (arrowheads) at day 7. **k**, Microvessel density at day 7 ($n = 4$; paired two-tailed *t*-test). Data are mean ± s.e.m.; *n* are independent animals (**g**,**i**,**k**); $^*P \le 0.05$, $^{**}P \le 0.01$, $^{***}P \le 0.001$. Scale bars, 50 nm (**a**); 10 µm (**b**,**c**); 50 µm (**f**); 100 µm (**j**). Related results in Extended Data Fig. 10.

mitochondrial donor MSCs (sh*PINK1*-MSCs). Silencing *ULK1*, a central enzyme in autophagy, in ECs served as a control. When the PINK1–Parkin-dependent mitophagy pathway was impaired, mitochondrial transplantation did not enable the engraftment of mitoAT-ECs into immunodeficient mice (Fig. 5e–g). Grafts with abrogated mitophagy showed a significantly reduced presence of perfused vessels at day 7 (Fig. 5g). By contrast, control mitoAT-ECs exhibited robust engraftment in the form of perfused blood vessels. Mechanistically, these results confirmed that the PINK1–Parkin pathway mediates mitophagy, which, in turn, regulates the enhanced engraftment ability shown by mitoAT-ECs after mitochondrial transplantation (Fig. 5h).

Mitophagy also had a role in regulating the engraftment ability of ECs when supported by MSCs. Vascularization at day 7 in grafts containing ECs and MSCs was significantly reduced when using either sh*PRKN*-ECs or sh*PINK1*-MSCs (Fig. 5i–k), confirming that mitophagy is implicated in regulating the engraftment of ECs in the co-implantation model.

Discussion

The role of mitochondrial transfer as a form of cell-to-cell signalling in health and disease is an area of active investigation. Studies have shown that mitochondrial transfer between different cell types—including the transfer from MSCs to lung alveolar epithelial cells and astrocytes to neurons—is crucial for tissue repair[8,9]. These studies reported a significant increase in ATP production in the recipient cells, suggesting the functional incorporation of exogenous mitochondria into the recipient pool of endogenous mitochondrial. However, the underlying mechanisms remain elusive, and understanding how a small number

of exogenous mitochondria could produce such substantial beneficial effects has been challenging.

In this study, we show that mitochondrial transfer serves as a mode of cell-to-cell communication in the vascular system. Under stressful conditions, such as during cell transplantation, perivascular MSCs transiently transferred mitochondria to neighbouring ECs through TNTs, enhancing their bioenergetics and overall fitness, and particularly their engraftment ability. Surprisingly, the process did not depend on transferring functional mitochondria. Enhanced EC engraftment was also observed after transferring mitochondria previously rendered dysfunctional by either Ca^{2+}-overload-mediated depolarization or mtDNA degradation. Mechanistically, once internalized, the exogenous mitochondria triggered mitophagy through the canonical PINK1–Parkin signalling pathway and were rapidly degraded in autophagosomes. Activation of mitophagy mediated the observed beneficial effects in recipient ECs, which were completely abrogated by blocking PINK1–Parkin signalling. These findings offer the first insights into a potential mechanism regulating the effects produced by mitochondrial transfer. The transferred mitochondria serve as a trigger for mitophagy and do not require functional competence, which explains how a few exogenous mitochondria could contribute significantly to ATP production in recipient cells.

The acquisition of mitochondria by ECs from diverse cellular sources has emerged as a topic of considerable interest. For instance, one report showed how MSCs can salvage injured ECs in an ischaemia-reperfusion model through TNT-mediated mitochondrial transfer[18]. More recently, a study provided evidence of the therapeutic potential of transplanting MSC-derived mitochondria, observing enhanced cardiac function after infarction by mitigating EC senescence[19]. Another team documented how the systemic release of mitochondria from adipocytes supported the metabolic adaptation of distant organs under nutrient stress, with ECs serving as major recipients of the exogenous mitochondria[20]. Further studies are warranted to determine whether the transient activation of mitophagy, as seen in our findings, also mediates the beneficial effects described after mitochondrial transfer in all of these other settings, as well as in other cellular systems beyond the vasculature.

Our study was at first focused on the TNT-mediated transfer mechanism, an intriguing natural process of cell-to-cell communication. However, from a translational standpoint, the natural transfer of mitochondria from MSCs to ECs poses some challenges. For instance, the co-culture set-up required for TNT-mediated transfer results in only about 25% of ECs receiving mitochondria over a 24-h period. Moreover, the process would necessitate an extra step to separate the ECs that received the exogenous mitochondria from the unprimed ECs. Given these limitations, we sought a more direct, efficient and potentially translational approach—hence the switch to artificial mitochondrial transplantation. Indeed, in addition to natural transfer from MSCs, we showed that artificial transplantation of exogenous mitochondria could also trigger mitophagy in ECs, resulting in similar cytoprotective effects, including an enhanced engraftment capability.

Mechanistically, the process of internalization of mitochondria during the natural transfer (through TNTs) differs from that in artificial transplantation (endocytosis). Nonetheless, we show that both the endocytic process and the TNT-mediated transfer converge on a shared functional outcome: activation of mitophagy and, in turn, cytoprotective effects in recipient ECs. For artificial transplantation, this would imply that a portion of the internalized mitochondria must escape from endosomal compartments to become accessible to cytoplasmic PINK1–Parkin pathways[21]. Evidence for such an endosomal escape includes the fact that silencing Parkin in recipient ECs (sh*PRKN*-ECs) significantly diminishes LC3B assembly and $LC3B^+$ autophagosome formation in mitoAT-ECs. Also, approximately 23% of DsRed-labelled exogenous mitochondria co-localized with cytoplasmic Parkin in mitoAT-ECs 24 h after mitochondria transplantation, corroborating the notion of partial endosomal escape. Although various escape mechanisms, such as endosomal membrane fusion and pH-dependent processes, have been proposed, the specifics are still under active investigation[21].

Mitochondrial transplantation has gained relevance as a potential treatment for several diseases, including cancer[22], Parkinson's disease[23] and myocardial infarction[24]. The beneficial effects observed in preclinical models led to a first-in-human study in children with myocardial ischaemia, which showed promising results[25]. However, the mechanisms of action by which the in-vivo-transplanted mitochondria amplify bioenergetics in recipient cells remain debated[26,27], and the specific effects of mitochondrial transplantation in ECs have not been examined.

In previous studies, there were two main points of contention concerning the mechanism underlying mitochondrial transplantation: (1) uncertainty about whether mitochondria could survive and retain activity throughout the transplantation process; and (2) scepticism about how a low number of transplanted mitochondria could significantly increase ATP in the recipient cells[26,27]. Nevertheless, our findings suggest a possible mechanism that could reconcile these concerns. First, we showed that the exogenous mitochondria did not need to remain functional and merely served as a trigger of mitophagy once internalized into the recipient cells. Indeed, all depolarized, Ca^{2+}-overloaded and even mtDNA-free mitochondria could effectively trigger mitophagy in ECs. After internalization, the exogenous mitochondria were always rapidly degraded in autophagosomes and thus did not incorporate into the endogenous mitochondrial pool in any notable way.

Second, because they act as triggering agents, the number of mitochondria required to activate mitophagy can be minuscule. We showed that even a minimal dose of one mitochondrion per cell equivalent could produce a 40% increase in the levels of ATP in 24 h (Extended Data Fig. 6h). Moderate mitophagy can benefit cells by virtue of degrading dysfunctional mitochondria and replacing them with new organelles through mitochondrial biogenesis[28], which ultimately translates into a meaningful increase in ATP. Indeed, once mitophagy was triggered in ECs, the expression of genes that mediate mitochondrial biogenesis (for example, *PPARGC1B*, *TMEM59*, *GFM1* and *TEAD4*) was significantly upregulated, and the total mitochondrial content was significantly increased, followed by a marked increase in ATP production. In short, we showed that the internalization of a small number of nonfunctional mitochondria could effectively trigger mitophagy and have substantial beneficial effects on the receiving ECs. Future studies should ascertain whether mitophagy is also the underlying mechanism behind the beneficial effects that have been described in other mitochondrial transplantation applications. Moreover, future studies to investigate activating mitophagy through alternative means, including the use of small chemicals or FDA-approved pharmacological agents known for their mitophagy-enhancing capabilities, are warranted.

Our study highlights the cytoprotective influence of mitophagy on EC function, and offers a plausible explanation for other observations in mitochondrial transplantation research. The safeguarding role of mitophagy across diverse cells and tissues is well-established, with its main function being the removal of malfunctioning mitochondria to ensure a stable intracellular equilibrium[29]. Furthermore, increasing evidence suggests that mitophagy stands as an acute response to tissue stress[30,31], preserving the integrity of the mitochondrial framework. Previous investigations have highlighted the MSC-specific induction of cytoprotective effects in various cells through mitophagy activation[32,33], including mitigating damages caused by hyperglycaemia in ECs through PINK1–Parkin-mediated mitophagy[34]. In light of our findings, these insights underline the essential role of mitophagy and position it as a promising therapeutic avenue in vascular research.

It is important to note that we focused mainly on the interaction between cells with competent mitochondrial respiration. In this scenario, we showed that the assimilation of exogenous mitochondria into the mitochondrial pool of receiving cells is minimal. However, previous studies have shown that when exogenous mitochondria are introduced

to cells with compromised mitochondrial function (for example, Rho^0 cells or *Ndufs4*$^{-/-}$ macrophages), there could be a selective advantage that is likely to promote the integration and amplification of competent donor mtDNA[20,35]. In these contexts, the exogenous mitochondria were shown to rectify inherent defects in aerobic respiration, as the competent donor mtDNA takes precedence. Thus, in scenarios in which endogenous mitochondrial function is deficient, the persistence and role of exogenous mitochondria might diverge from our observations.

Our studies have direct translational implications. We showed that ex vivo artificial mitochondrial transplantation could effectively improve the engraftment capacity of ECs in ischaemic tissues, in which they form new blood vessels and provide robust therapeutic effects without the need for other cell types. The reliance on a single cell type simplifies clinical translation enormously. We anticipate that our mitochondrial transplantation approach could become the basis for a new strategy in vascular cell therapies. Whether this strategy could benefit other forms of cell therapies remains to be determined.

Online content

Any methods, additional references, Nature Portfolio reporting summaries, source data, extended data, supplementary information, acknowledgements, peer review information; details of author contributions and competing interests; and statements of data and code availability are available at https://doi.org/10.1038/s41586-024-07340-0.

1. Nowbar, A. N., Gitto, M., Howard, J. P., Francis, D. P. & Al-Lamee, R. Mortality from ischemic heart disease. *Circ. Cardiovasc. Qual. Outcomes* **12**, e005375 (2019).
2. Loffredo, F. & Lee, R. T. Therapeutic vasculogenesis. *Circ. Res.* **103**, 128–130 (2008).
3. Melero-Martin, J. M. et al. Engineering robust and functional vascular networks in vivo with human adult and cord blood-derived progenitor cells. *Circ. Res.* **103**, 194–202 (2008).
4. Beckman, J. A., Schneider, P. A. & Conte, M. S. Advances in revascularization for peripheral artery disease: revascularization in PAD. *Circ. Res.* **128**, 1885–1912 (2021).
5. Carmeliet, P. & Jain, R. K. Molecular mechanisms and clinical applications of angiogenesis. *Nature* **473**, 298 (2011).
6. Cooke, J. P. & Losordo, D. W. Modulating the vascular response to limb ischemia. *Circ. Res.* **116**, 1561–1578 (2015).
7. Wang, K., Lin, R.-Z. & Melero-Martin, J. M. Bioengineering human vascular networks: trends and directions in endothelial and perivascular cell sources. *Cell. Mol. Life Sci.* **76**, 421–439 (2019).
8. Islam, M. N. et al. Mitochondrial transfer from bone-marrow–derived stromal cells to pulmonary alveoli protects against acute lung injury. *Nat. Med.* **18**, 759 (2012).
9. Hayakawa, K. et al. Transfer of mitochondria from astrocytes to neurons after stroke. *Nature* **535**, 551 (2016).
10. Jain, R. K. Molecular regulation of vessel maturation. *Nat. Med.* **9**, 685–693 (2003).
11. Andrae, J., Gallini, R. & Betsholtz, C. Role of platelet-derived growth factors in physiology and medicine. *Gene Dev.* **22**, 1276–1312 (2008).
12. Rustom, A., Saffrich, R., Markovic, I., Walther, P. & Gerdes, H.-H. Nanotubular highways for intercellular organelle transport. *Science* **303**, 1007–1010 (2004).
13. Zhang, Y. et al. iPSC-MSCs with high intrinsic MIRO1 and sensitivity to TNF-α yield efficacious mitochondrial transfer to rescue anthracycline-induced cardiomyopathy. *Stem Cell Rep.* **7**, 749–763 (2016).
14. Hase, K. et al. M-Sec promotes membrane nanotube formation by interacting with Ral and the exocyst complex. *Nat. Cell Biol.* **11**, 1427–1432 (2009).
15. Kitani, T., Kami, D., Matoba, S. & Gojo, S. Internalization of isolated functional mitochondria: involvement of macropinocytosis. *J. Cell. Mol. Med.* **18**, 1694–1703 (2014).
16. Youle, R. J. & Narendra, D. P. Mechanisms of mitophagy. *Nat. Rev. Mol. Cell Biol.* **12**, 9–14 (2011).
17. Jin, S. M. & Youle, R. J. PINK1- and Parkin-mediated mitophagy at a glance. *J. Cell Sci.* **125**, 795–799 (2012).
18. Liu, K. et al. Mesenchymal stem cells rescue injured endothelial cells in an in vitro ischemia–reperfusion model via tunneling nanotube like structure-mediated mitochondrial transfer. *Microvasc. Res.* **92**, 10–18 (2014).
19. Liang, X. et al. Direct administration of mesenchymal stem cell-derived mitochondria improves cardiac function after infarction via ameliorating endothelial senescence. *Bioeng. Transl. Med.* **8**, e10365 (2023).
20. Borcherding, N. et al. Dietary lipids inhibit mitochondria transfer to macrophages to divert adipocyte-derived mitochondria into the blood. *Cell Metab.* **34**, 1499–1513 (2022).
21. Kami, D. & Gojo, S. From cell entry to engraftment of exogenous mitochondria. *Int. J. Mol. Sci.* **21**, 4995 (2020).
22. Elliott, R. L., Jiang, X. P. & Head, J. F. Mitochondria organelle transplantation: introduction of normal epithelial mitochondria into human cancer cells inhibits proliferation and increases drug sensitivity. *Breast Cancer Res. Treat.* **136**, 347–354 (2012).
23. Chang, J.-C. et al. Allogeneic/xenogeneic transplantation of peptide-labeled mitochondria in Parkinson's disease: restoration of mitochondria functions and attenuation of 6-hydroxydopamine–induced neurotoxicity. *Transl. Res.* **170**, 40–56 (2016).
24. Kaza, A. K. et al. Myocardial rescue with autologous mitochondrial transplantation in a porcine model of ischemia/reperfusion. *J. Thorac. Cardiovasc. Surg.* **153**, 934–943 (2017).
25. Emani, S. M., Piekarski, B. L., Harrild, D., Del Nido, P. J. & McCully, J. D. Autologous mitochondrial transplantation for dysfunction after ischemia-reperfusion injury. *J. Thorac. Cardiovasc. Surg.* **154**, 286–289 (2017).
26. Bertero, E., Maack, C. & O'Rourke, B. Mitochondrial transplantation in humans: "magical" cure or cause for concern? *J. Clin. Invest.* **128**, 5191–5194 (2018).
27. Lightowlers, R. N., Chrzanowska-Lightowlers, Z. M. & Russell, O. M. Mitochondrial transplantation—a possible therapeutic for mitochondrial dysfunction? *EMBO Rep.* **21**, e50964 (2020).
28. Ashrafi, G. & Schwarz, T. L. The pathways of mitophagy for quality control and clearance of mitochondria. *Cell Death Differ.* **20**, 31–42 (2013).
29. Moreau, K., Luo, S. & Rubinsztein, D. C. Cytoprotective roles for autophagy. *Curr. Opin. Cell Biol.* **22**, 206–211 (2010).
30. Gao, Y. et al. Role of Parkin-mediated mitophagy in the protective effect of polydatin in sepsis-induced acute kidney injury. *J. Transl. Med.* **18**, 114 (2020).
31. Livingston, M. J. et al. Clearance of damaged mitochondria via mitophagy is important to the protective effect of ischemic preconditioning in kidneys. *Autophagy* **15**, 2142–2162 (2019).
32. Sun, Z. et al. MSC-derived extracellular vesicles activate mitophagy to alleviate renal ischemia/reperfusion injury via the miR-223-3p/NLRP3 axis. *Stem Cells Int.* **2022**, 6852661 (2022).
33. Mahrouf-Yorgov, M. et al. Mesenchymal stem cells sense mitochondria released from damaged cells as danger signals to activate their rescue properties. *Cell Death Differ.* **24**, 1224–1238 (2017).
34. Zhu, W. et al. Mesenchymal stem cells ameliorate hyperglycemia-induced endothelial injury through modulation of mitophagy. *Cell Death Dis.* **9**, 837 (2018).
35. Kim, M. J., Hwang, J. W., Yun, C.-K., Lee, Y. & Choi, Y.-S. Delivery of exogenous mitochondria via centrifugation enhances cellular metabolic function. *Sci. Rep.* **8**, 3330 (2018).

Methods

Cell culture

Human ECFCs, herein referred to as ECs, and MSCs were isolated from human umbilical cord blood and subcutaneous adipose tissue, respectively, in accordance with established protocols[36,37]. ECs were cultured on plates pre-coated with 1% (w/v) gelatin and sustained in endothelial cell medium comprising EGM2 (lacking hydrocortisone; PromoCell), enriched with 20% fetal bovine serum (FBS; Hyclone), and 1× glutamine–penicillin–streptomycin (GPS; Invitrogen). MSCs were cultured in uncoated plates using mesenchymal stem cell growth medium (MSCGM; ATCC), supplemented with MSC growth supplement (ATCC) and 1× GPS. For all experiments, ECs and MSCs at passages 6 through to 12 were used.

Generation of mitoDsRed-labelled cells

MitoDsRed-labelled cells were produced by transfecting either ECs or MSCs with a piggyBac transposon vector. This vector contains a cytomegalovirus (CMV) promoter-driven DsRed reporter gene, which is fused to a mitochondrial targeting sequence derived from cytochrome C oxidase (mitoDsRed). In addition, a super piggyBac transposase expression vector (System Biosciences) was used. A ratio of 5:1 transposon to transposase vectors was used for the transfection, with a total of 2.4 μg of DNA for 1×10^6 cells. After transfection, cells underwent hygromycin selection, facilitating stable expression of the mitoDsRed reporter gene. This allowed for effective mitochondrial visualization under fluorescence microscopy. In specific experiments, MitoTracker Green FM Special Packaging (Thermo Fisher Scientific, M7514) was used for visualizing total mitochondria.

Generation of mitoAPEX2-labelled MSCs

MSCs were transfected with a piggyBac transposon system to generate mitochondrial-specific APEX2 labelling. The system comprised a vector carrying a CMV promoter-driven *APEX2* gene, fused with a mitochondrial targeting sequence derived from cytochrome C oxidase (mitoAPEX2), along with a super piggyBac transposase expression vector (System Biosciences). A ratio of 5:1 for the transposon to transposase vectors was used, with 2.4 μg of DNA for the transfection of 1×10^6 cells. After hygromycin selection, stable expression of the mitoAPEX2 reporter gene was attained. For visualizing the activity of APEX2 by TEM, the cells were chemically fixed and stained with 3,3′-diaminobenzidine (DAB) and hydrogen peroxide (H_2O_2) for 15 min, followed by processing for TEM using heavy-metal staining. This DAB staining technique provided enhanced contrast of the mitochondrial matrix in the transfected cells.

In vitro mitochondrial transfer by co-culture

Co-culture experiments involved human ECs and mitoDsRed-labelled MSCs on 1% gelatin-coated plates in EC medium. The effect of cell density on mitochondrial transfer was assessed by co-culturing mitoDsRed-MSCs and ECs in a 1:1 ratio, with total cell numbers ranging from 0.05×10^6 to 0.8×10^6 per well. Different donor-to-recipient ratios, from 1:10 to 10:1, were also evaluated, keeping the total cell count at 4×10^5 per well. The effects of environmental conditions were studied by co-culturing mitoDsRed-MSCs and ECs at a 1:1 ratio, with 4×10^5 total cells, in either two-dimensional (2D) or 3D (collagen hydrogel) conditions, under normoxia (21% O_2) or hypoxia (1% O_2). After 24 h, analysis was performed by microscopy and flow cytometry. Selected experiments examined the effects of VEGF (10 ng ml^{-1}), bFGF (10 ng ml^{-1}), TNF (10 ng ml^{-1}), anti-TNF antibody (10 ng ml^{-1}), IL-1α (20 ng ml^{-1}), IL-1β (20 ng ml^{-1}) and anti-IL-1α antibody (10 ng ml^{-1}) on mitochondrial transfer and TNT formation.

Immunofluorescence staining

Cells were seeded at 60,000 cells per cm^2 in eight-well LAB-TEK chamber slides. After reaching confluency, they were fixed with 4% paraformaldehyde (PFA), permeabilized using 0.1% Triton X-100 in PBS and blocked for 30 min with 5% horse serum (Vector Laboratories, S-2000). Incubation with primary antibodies, including LC3B (Cell Signaling, 2775), β-actin (Abcam, 8226) and α-tubulin (EP1332Y; Abcam, ab52866), was performed for 30 min at room temperature. This was followed by three PBS washes and a 30-min incubation with secondary antibodies at room temperature. Cells were then washed three times with PBS and stained with DAPI (0.5 μg ml^{-1}) for 5 min. The slides were finally mounted using DAKO fluorescence mounting medium (Agilent, S302380-2).

Flow cytometry and cell sorting

Cells were stained for flow cytometry and analysed with a Guava easyCyte 6HT/2L flow cytometer (Millipore Corporation) and FlowJo software (Tree Star). Antibody labelling was performed on ice for 20 min, followed by three washes with PBS (1% bovine serum albumin (BSA) and 0.2 mM EDTA) and fixation with 1% PFA. Antibodies included PE-conjugated anti-human CD90 (BD Biosciences, 555596), APC-conjugated anti-human CD90 (eBioscience, 17-0909-41) and FITC-conjugated anti-human CD31 (BD Biosciences, 555445). In indicated experiments, cells were retrieved from explanted grafts before flow cytometry analysis. Grafts were removed from euthanized mice, and cells were retrieved by enzymatic digestion (1 mg ml^{-1} collagenase and 2.5 U ml^{-1} dispase) for 1 h at 37 °C. Cells were prepared into single-cell suspensions. When indicated, cells were sorted into hCD31$^+$ and hCD31$^-$ cells using magnetic-activated cell sorting with anti-human CD31 antibody-coated magnetic beads (DynaBead). In indicated experiments, cells were sorted into hCD31$^+$mitoDsRed$^+$ (mitoT-ECs) and hCD31$^+$mitoDsRed$^-$ (unprimed ECs) using fluorescence-activated cell sorting (FACS) with a FACSMelody sorter system (BD Bioscience). Rabbit anti-PINK1 (Thermo Fisher Scientific, PA5-86941) was used for the detection of PINK1 proteins in the presence of isolated mitochondria.

Animal experiments

Animal experiments were approved by the Institutional Animal Care and Use Committee at Boston Children's Hospital and were performed in an AAALAC-approved facility. Mice were housed under a 12-h dark–light cycle, with the ambient temperature maintained at 20–23 °C and the relative humidity at 30–70%. Sample size, including the number of mice per group, was determined to ensure adequate power and was based on the means and variations observed in our pilot experiments and historical data. No data were excluded. No exclusion criteria were applied for all analyses. Mice were randomly selected and allocated to groups for each type of experiment. There was no expected outcome before the analysis, and blinding was not relevant.

In vivo cell engraftment

Human ECs (8×10^5 cells) were resuspended in 200 μl ice-cold collagen–fibrin–laminin hydrogel solution containing bovine collagen I (1.5 mg ml^{-1}; Trevigen), fibrinogen (3 mg ml^{-1}), laminin-1 (2 mg ml^{-1}), FGF-2 (1 μg ml^{-1}; PeproTech), and erythropoietin (5 μg ml^{-1}; ProSpec), with or without MSCs (1.2×10^6 cells). The mixture was subcutaneously injected into six-week-old male athymic nu/nu mice (Massachusetts General Hospital). During anaesthesia, mice received 50 μl of thrombin (10 U ml^{-1}; Sigma-Aldrich) subcutaneously before 200 μl of cell-laden hydrogel solution. Supplements added to the cell–hydrogel mixture as needed were VEGF-A (R&D Systems; 100 ng per implant), bFGF (50 ng per implant), the PDGFR inhibitor tyrphostin AG1296 (Sigma; 1.33 μg per implant) or concentrated MSC-conditioned medium (100 μl per implant). Conditioned media were generated by 1.2×10^6 MSCs in EBM-2 and 5% FBS, and were concentrated tenfold. Mice were euthanized, and grafts were explanted at different time points. Previously, we have shown that grafts contain human ECs and MSCs for at least four weeks[37]. In some experiments, rhodamine-conjugated UEA1 lectin (Vector Laboratories; 100 μl; 1 mg ml^{-1} in saline) was injected intravenously before

collection. In others, TNF or saline were injected into EC–MSC implants on day 14, with grafts explanted on day 16.

Mouse hindlimb ischaemia model

Immune-deficient athymic nu/nu nude mice (10 weeks old; male) were induced diabetic with a single intraperitoneal injection of streptozotocin (STZ; 220 mg per kg) and had their blood glucose levels monitored after two days. Seven days after STZ injection, diabetic mice were anaesthetized using isoflurane. Once anaesthesia was achieved, 7-0 silk sutures were tied around the proximal and deep femoral artery and vein, and the vessels between the ties were cut to completely block blood flow. ECs (2×10^6) were resuspended in 50 µl ice-cold Phenol Red-free Matrigel (BD Biosciences) and injected into the muscle where the femoral artery and vein ligation occurred.

Laser Doppler imaging

Blood flow in hindlimbs was analysed using the LDI2-IR laser Doppler blood flow imager (Moor Instruments). Imaging was performed before surgery and on post-operative days 0, 1, 3, 5, 7, 10, 14 and 28. The relative changes in blood flow in the hindlimbs were expressed as the ratio of the operated hindlimb to the blood flow in the contra-lateral (opposite) hindlimb, using the company's software.

Bioluminescence imaging

Lucif-ECs were generated by transfection with a PiggyBac vector carrying a CMV promoter-driven firefly luciferase reporter gene and a super PiggyBac transposase expression vector (System Biosciences) or lentivirus transduction. A 5:1 ratio between transposon and transposase vectors was used, with 2.4 µg of DNA for 1×10^6 ECs. Puromycin-selected lucif-ECs showed stable luciferase expression. Lucif-ECs (8×10^5 cells) were resuspended in 200 µl ice-cold collagen–fibrin–laminin hydrogel, with or without MSCs (1.2×10^6 cells), and were subcutaneously injected into six-week-old male athymic nu/nu mice. Mice were imaged at 0.5 h and on days 1, 3, 7, 14 and 28 after injection using an IVIS 200 Imaging System (Xenogen Corporation). Mice were anaesthetized, and luciferin (Promega) was injected intraperitoneally (125 mg per kg). Bioluminescence was detected 5 min after luciferin administration, and data were analysed using Live Image 3.0 (Xenogen Corporation).

Histology and immunofluorescence staining

Explanted grafts were fixed overnight in 10% buffered formalin, paraffin-embedded and sectioned (7 µm). Haematoxylin and eosin (H&E)-stained sections were examined for erythrocyte-filled blood vessels. For immunostaining, sections underwent deparaffinization, antigen retrieval with tris-EDTA buffer (10 mM Tris-Base, 2 mM EDTA and 0.05% Tween-20, pH 9.0) or citric buffer (10 mM sodium citrate and 0.05% Tween-20, pH 6.0), blocking with 5–10% serum and overnight incubation at 4 °C with primary antibodies. Fluorescent staining used fluorescently conjugated secondary antibodies (1:200) and DAPI counterstaining (Vector Laboratories). Human-specific anti-CD31 antibody (Agilent; M082329-2 J; clone JC70A), human-specific vimentin antibody (Abcam; Ab8069; clone V9) and *Ulex europaeus* agglutinin I (UEA-I; Vector Laboratories) stained human blood vessels. Perivascular cells were stained by anti-α-SMA antibody (Sigma; A2547; clone 1A4).

Microvessel density

Microvessel density was calculated as the average number of erythrocyte-filled vessels (vessels per mm^2) in H&E-stained sections from implant centres. The entire area of each section was analysed. Human-specific microvessel density was quantified in indicated experiments using hCD31-immunostained slides.

Silencing of gene expression by shRNA

shRNA lentiviral particles targeting human *TNFAIP2*, *MIRO1*, *PRKN* and *PINK1*, along with negative control shRNA constructs, were obtained from Santa Cruz Biotechnology. Cells (5×10^5) were transduced with shRNA lentiviral particles (multiplicity of infection of 10:1) and polybrene (5 µg per ml). After 48 h, cells were selected with 1 µg ml^{-1} puromycin. mRNA was isolated from transfected cells, and quantitative PCR with reverse transcription (qRT–PCR) was performed to validate the shRNA silencing efficiency.

Mitochondria isolation and artificial transfer

Mitochondria were isolated from donor cells using the Mitochondria Isolation Kit for Cultured Cells (Thermo Fisher Scientific). Cells were collected with trypsin, washed twice with cold PBS and resuspended in 800 µl of buffer A with 10 µl of Mitochondria Isolation Reagent B. After a 5-min incubation on ice with intermittent vortexing, 800 µl of buffer C was added, and the cell suspension was homogenized with a Dounce tissue grinder. After centrifugation at 700*g* for 10 min at 4 °C, the supernatant was transferred to a new tube and centrifuged at 12,000*g* for 15 min at 4 °C. The isolated mitochondrial pellet was resuspended in 500 µl buffer C with 1% BSA and then centrifuged at 3,000*g* for final purification. For artificial mitochondrial transfer, isolated mitochondria were mixed with EC medium and added to ECs in culture at a 3:1 donor-to-recipient cell ratio. For titration experiments, the number of isolated mitochondria was quantified using flow cytometry (FACSAria II 5-LASER sorter system) and then transferred at various mitochondria-to-cell ratios, including 1×, 2×, 4×, 8×, 16×, 32× and 64× mitochondria per cell. After 12 h of mitochondrial transplantation, the plates were washed twice with PBS, and cells were maintained in culture in EC medium.

Isolation of lysosomes and artificial transfer

Lysosomes were isolated by differential sedimentation from supernatants derived after mitochondrial isolation and purification (3,000*g*). To eliminate residual mitochondria, these supernatants were sequentially filtered through sterile syringe filters of 0.8 µm and 1.2 µm pore size (Millipore Sigma). Lysosomes were then collected by centrifugation at 20,000*g*. For the final purification step, the isolated lysosomes were resuspended in 500 µl of buffer C containing 1% BSA, and subjected to centrifugation at 3,000*g*. The artificial transfer of lysosomes to ECs was performed by mixing isolated lysosomes with EC culture medium and adding them to EC cultures at a 3:1 donor-to-recipient cell ratio. After a 12-h lysosomal transplantation period, the cell cultures were washed twice with PBS and subsequently maintained in EC medium.

Quantitative analysis of exogenous mitochondria and Parkin co-localization

ECs, after 12-h DsRed-mitochondrial transplantation, were fixed using ice-cold methanol at 4 °C. Permeabilization was achieved with 0.1% Triton X-100 in PBS, followed by blocking in 5% horse serum (Vector Laboratories) for 1 h. Overnight incubation at 4 °C was then performed with the anti-Parkin antibody (Abcam, ab77924). After three PBS washes, cells were incubated with appropriate secondary antibodies at room temperature for 1 h. After another three PBS washes, nuclear staining was performed using DAPI for 15 min. A quantitative assessment of Parkin and mitochondrial fluorescence was conducted with ImageJ on the basis of pixel coloration metrics: Parkin (yellow), mitochondria (red) and their co-localization (orange).

JC-10 fluorescent assay for measuring mitochondrial membrane potential

Depolarization of isolated mitochondria was evaluated with the JC-10 fluorescent assay for mitochondrial membrane potential (Enzo Life Sciences, ENZ-52305) according to the manufacturer's instructions. Isolated mitochondria were assessed immediately after isolation in Ca^{2+}-containing (around 1.6 mM) EGM2 medium and Ca^{2+}-free C buffer. The fluorescent intensities for aggregate (red FL, 590 nm) and monomeric (green FL, 520 nm) forms of JC-10 were measured at

Ex/Em = 490/590 nm and 490/520 nm with a microplate reader. The percentage of membrane potential was represented as the FL_{590}/FL_{520} ratio.

Migration assay

The scratch assay was conducted on confluent ECs in a six-well plate. Scratch wounds were created using a 1,000-µl pipette tip, and artificial mitochondrial transfer was performed immediately. The scratch size was measured after 12 h for each condition.

Apoptosis assay

Confluent ECs were treated with 0.2 mM H_2O_2 for 12 h, with or without artificial mitochondrial transfer. Apoptosis was assessed using APC-conjugated Annexin V and propidium iodide (PI) staining (Annexin V Apoptosis Detection Kit; eBioscience) by flow cytometry, following the manufacturer's instructions.

ATP measurement

Confluent ECs were treated with artificial mitochondrial transfer or control for 24 h. Total cellular ATP was measured using the Luminescent ATP Detection Assay Kit (Abcam, ab113849) according to the manufacturer's instructions.

Bioenergetics assessment

Bioenergetics changes resulting from artificial mitochondrial transfer in ECs were investigated by measuring the oxygen consumption rate (OCR) using a Seahorse XFe96 Analyzer. ECs were plated at various seeding densities to determine the optimal density of 30,000 cells per well. Optimal drug concentrations were 1.5 µmol l^{-1} for oligomycin, 1 µmol l^{-1} for FCCP and 1.25 µmol l^{-1} of rotenone + 2.5 µmol l^{-1} of antimycin A (R&A). Transferred mitochondria were co-incubated with ECs for 24 h before removing uninternalized mitochondria by changing the medium. Seahorse assays were conducted in Seahorse XF DMEM supplemented with 10 mmol l^{-1} glucose, 1 mmol l^{-1} sodium pyruvate and 2 mmol l^{-1} L-glutamine. OCR measurements were performed with the sequential treatment of oligomycin, FCCP and R&A following the Seahorse XFe96 Analyzer program.

RNA-seq analysis

The following groups were analysed: unprimed ECs, mitoT-ECs and mitoAT-ECs. Each group consists of at least two biological replicates. Total RNA was extracted using the RNeasy Mini Kit (Qiagen) following the manufacturer's protocol. RNA quantity and quality were checked with NanoDrop and Agilent Bioanalyzer. Libraries were prepared and sequenced by Genewiz using the Illumina HiSeq 2500 platform (Illumina) with 2 × 150 paired-end configurations. The raw reads were quality controlled (FastQC) and trimmed. Reads were then aligned to the UCSC hg38 genome (STAR aligner), and transcript expression was calculated by Salmon. The reference genome (hg38.fa.gz) and genome annotation file (hg38.knownGene.gtf.gz) are both publicly available from the UCSC Genome Browser (https://genome.ucsc.edu/cgi-bin/hgGateway). Pairwise comparisons of differentially expressed (DE) genes were performed by DESeq2 (v.1.38.1, threshold used: fold change > 2, $P < 0.05$). Intersected combined DE genes were subjected to heat map and PCA plotting (R v.4.2.1). DE genes upregulated in mitoT-ECs, and mitoAT-ECs groups against unprimed ECs, were annotated for GO analysis with the R package ClusterProfiler (v.4.6.2).

qPCR

Total RNA was extracted from cells using the RNeasy Mini Kit (Qiagen) following the manufacturer's instructions. RNA concentration and purity were measured using a NanoDrop 8000 spectrophotometer (Thermo Fisher Scientific), on the basis of the absorbance ratio at 260 nm and 280 nm. cDNA synthesis was performed using the High-Capacity RNA-to-cDNA Kit (Thermo Fisher Scientific). Quantitative PCRs were conducted on the QuantStudio 6 Flex Real-Time PCR System with PowerUp SYBR Green Master Mix (Thermo Fisher Scientific), using *GAPDH* as the housekeeping gene.

Human cytokine protein array

Selected cytokines were evaluated in conditioned medium samples using the Proteome Profiler Human Angiogenesis Array (R&D Systems, ARY007) as per the manufacturer's instructions. Antigen–antibody reactions were visualized with LumiGLO substrate (Kirkegaard & Perry Laboratories) and chemiluminescent-sensitive film (Kodak). Densitometry was performed using image analysis (ImageJ) to estimate protein amounts in each sample.

Western blot analysis

Mitochondrial and cellular lysates were prepared using radioimmunoprecipitation assay (RIPA) buffer (Millipore Sigma, R278). Protein concentrations were quantified using a bicinchoninic acid (BCA) assay (Thermo Fisher Scientific, 23227). Equal amounts of protein from each sample were resolved on Novex 4–12% Tris-Glycine gels (Thermo Fisher Scientific), and were subsequently transferred onto polyvinylidene fluoride (PVDF) membranes (Bio-Rad) using the Novex Mini-Cell XCell SureLock system (Invitrogen). Membrane blocking was performed with 5% non-fat milk powder in TBST for 1 h at room temperature, followed by incubation at 4 °C overnight with primary antibodies: rabbit anti-GAPDH (Sigma, G9545), rabbit anti-β-actin (ABclonal, AC038), rabbit anti-PINK1 (Novus Biological, BC100-494) and mouse anti-TOM20 (Abcam, ab56783). After thorough washing, membranes were incubated with horseradish peroxidase (HRP)-conjugated secondary antibodies. Protein bands were visualized using HRP-enhanced chemiluminescence (ECL) substrate (Kindle Biosciences, western blot detection kit, R1004).

mtDNA heteroplasmy

To assess the persistence of transferred mitochondria in recipient ECs over time, we used a mtDNA genotyping approach that relies on detecting heteroplasmy. mtDNA was isolated from cells using the Mitochondrial DNA Isolation Kit (Abcam, ab65321). PCR amplification of the hypervariable regions (HVR1 and HVR2) of mtDNA was performed using the following primers: (1) HVR1, primer name: A1 mitoPrimer (L15997) (amplicon size: 342 bp; primer sequence: 5′-CACCATTAGCACCCAAAGCT-3′) and primer name: B1 mitoPrimer (H16391) (amplicon size: 342 bp; primer sequence: 5′-GAGGATGGTGGTCAAGGGAC-3′); and (2) HVR2, primer name: C1 mitoPrimer (L048) (amplicon size: 268 bp; primer sequence: 5′-CTCACGGGAGCTCTCCATGC-3′) and primer name: D1 mitoPrimer (H408) (amplicon size: 268 bp; primer sequence: 5′-CTGTTAAAAGTGCATACCGCCA-3′). Then, Sanger sequencing was performed using the same primers to read the mtDNA sequences.

Split-GFP mitochondrial fusion assay

A split-GFP system strategy was adopted to determine whether transferred mitochondria fuse with the recipient's mitochondrial pool. In this system, GFP is split into two components, which only produce a fluorescent signal when both components are present. Two piggyBac transposon vectors were created, each encoding one of the two GFP components (components GFP-1–10 and GFP-11) fused with a mitochondrial targeting sequence from cytochrome C oxidase (referred to as mtGFP-1–10 and mtGFP-11). Mitochondrial donor mitoDsRed-MSCs were transduced with mtGFP-11, and recipient ECs were transduced with mtGFP-1–10. After natural or artificial mitochondrial transfer, green fluorescence is only observed if donor mitochondria fuse with the endogenous mitochondrial pool (that is, mtGFP-1–11). The fluorescence of isolated mitochondria was analysed by flow cytometry (BD FACS LSRFortessa).

mtDNA-free human MSC-ρ0 cells

A piggyBac transposon vector carrying a Dox-inducible GFP-EcoRI fusion protein that targets mitochondria was constructed. This vector

was co-transfected with a super piggyBac transposase vector into human mitoDsRed-MSCs and selected with 2 μg ml^{-1} puromycin. Stable engineered MSC lines were maintained in normal MSC medium. To induce mtDNA depletion, Dox (0.5 μg ml^{-1}) was added to activate the expression of the mitochondrially targeted GFP-EcoRI fusion protein, which led to the digestion of mtDNA. Depletion of mtDNA was confirmed after 3 days by qPCR. The resulting mtDNA-free human MSC-ρ0 cells were maintained in DMEM high glucose supplemented with GlutaMAX, pyruvate (110 μg ml^{-1}), 50 μg ml^{-1} uridine and 10% FBS. Control mtDNA-free EC-ρ0 cells were similarly generated and maintained in EGM2 supplemented with 20% FBS, GlutaMAX, 110 μg ml^{-1} pyruvate and 50 μg ml^{-1} uridine.

Autophagic flux analysis

MitoAT-ECs were cultured until they reached 80% confluency. Cells were then treated with 100 nM bafilomycin A1 for 3 h to inhibit autophagosome–lysosome fusion. Cells were lysed with RIPA buffer containing protease inhibitors, and protein concentration was determined using a BCA assay. A total of 30 μg of protein was separated on a 12% SDS–PAGE gel and transferred onto a nitrocellulose membrane. The membrane was blocked with 5% non-fat milk in TBST buffer for 1 h at room temperature and probed overnight at 4 °C with the primary antibody against LC3B (Abcam, ab51520) at a dilution of 1:1,000 in TBST buffer. The membrane was then washed three times with TBST buffer and incubated for 1 h at room temperature with HRP-conjugated secondary antibody. The immunoreactive bands were visualized using an enhanced chemiluminescence (ECL) detection system.

Microscopy

Images were captured using the Axio Observer Z1 inverted microscope (Carl Zeiss) and AxioVision Rel. 4.8 software. Fluorescent images were taken with an ApoTome.2 Optical sectioning system (Carl Zeiss) and a 20× or 40× objective lens. Non-fluorescent images were taken with an AxioCam MRc5 camera using a 10× or 20× objective lens.

Statistics and reproducibility

All experiments, including representative micrographs, were independently repeated at least three times. All statistical analyses were performed using GraphPad Prism v.7 software (GraphPad Software). The sample size, including the number of mice per group, was chosen to ensure adequate power and was based on historical laboratory data. No exclusion criteria were applied for all analyses. All data are expressed as mean ± s.e.m. Comparisons between multiple groups were performed by one-way ANOVA followed by Bonferroni's post-test. Unpaired two-tailed Student's *t*-test was used for comparisons between two groups. A value of $P < 0.05$ was considered to be statistically significant.

Reporting summary

Further information on research design is available in the Nature Portfolio Reporting Summary linked to this article.

Data availability

All data supporting the findings of this study are available in the paper and its Supplementary Information. The RNA-seq datasets generated during the study are available in the Gene Expression Omnibus repository, under the accession number GSE255798. Source data are provided with this paper.

36. Melero-Martin, J. M. et al. In vivo vasculogenic potential of human blood-derived endothelial progenitor cells. *Blood* **109**, 4761–4768 (2007).
37. Lin, R.-Z. et al. Human endothelial colony-forming cells serve as trophic mediators for mesenchymal stem cell engraftment via paracrine signaling. *Proc. Natl Acad. Sci. USA* **111**, 10137–10142 (2014).

Acknowledgements Illustrations were partially created with BioRender.com. This work was supported by a grant from the National Institutes of Health (NIH) (RO1HL152133 to J.M.M.-M.). Work in the N.P. laboratory was supported by a NIH NIAMS R01 grant.

Author contributions R.-Z.L. and J.M.M.-M. conceived and designed the project. R.-Z.L., G.-B.I., A.C.L., Y.Z., X.H., J.N. and H.-W.T. performed the experimental work. All authors discussed and analysed the data and edited the results. R.-Z.L. and J.M.M.-M. wrote the manuscript.

Competing interests The authors declare no competing interests.

Additional information

Supplementary information The online version contains supplementary material available at https://doi.org/10.1038/s41586-024-07340-0.

Correspondence and requests for materials should be addressed to Juan M. Melero-Martin.

Peer review information *Nature* thanks Jonathan Brestoff, Anna Randi and the other, anonymous, reviewer(s) for their contribution to the peer review of this work.

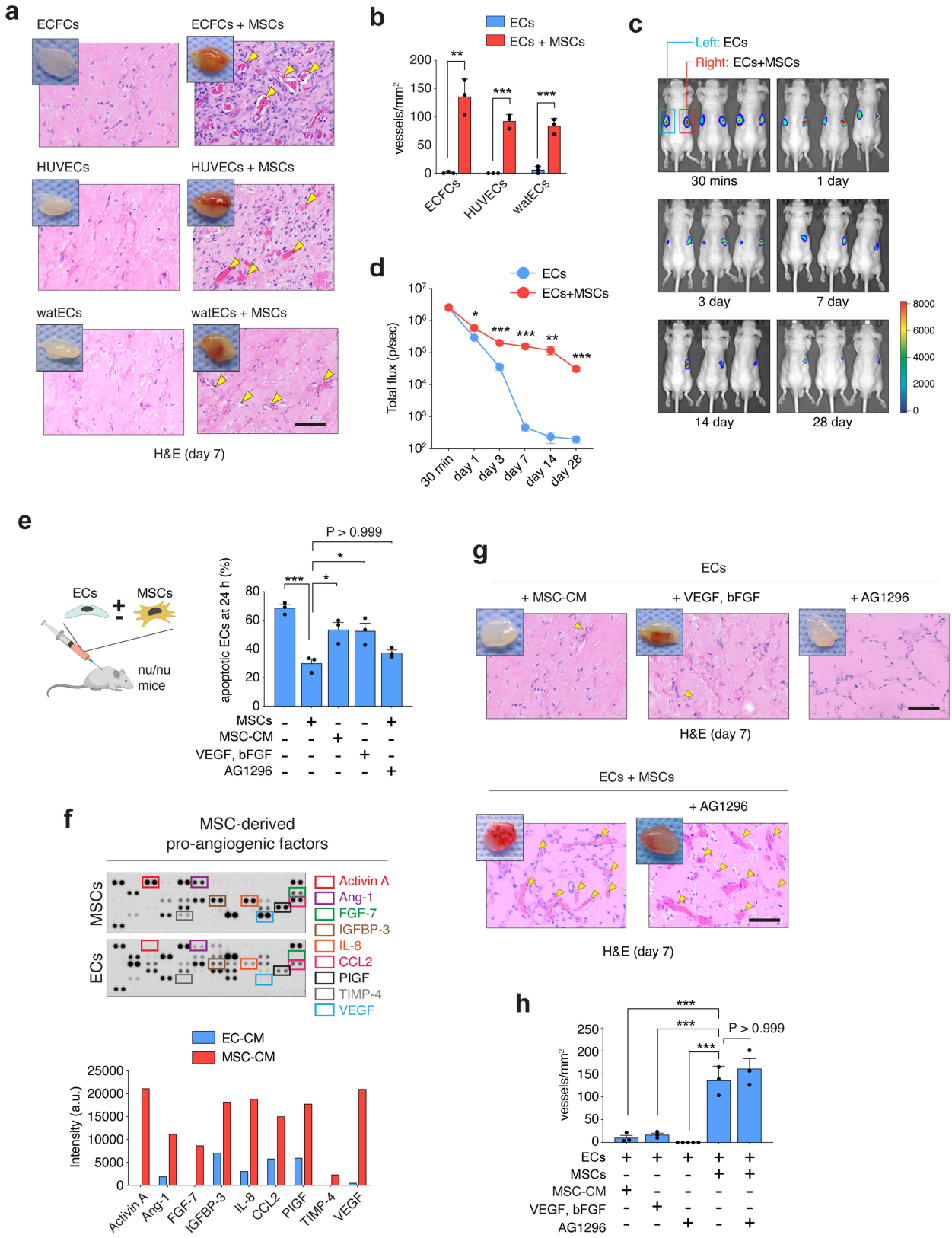

Extended Data Fig. 1 | Stromal cell support is essential for human EC engraftment. Grafts comprising human ECs with or without MSCs were subcutaneously implanted in immunodeficient nude mice. **a**, H&E staining of 7-day explants with human ECFCs, HUVECs, and wat-ECs, highlighting perfused vessels (yellow arrowheads). Insets show day 7 macroscopic views. Scale bar, 100 µm. **b**, Microvessel density at day 7 with various human EC types; $^{**}P \le 0.01$, $^{***}P \le 0.001$ (n = 3; unpaired t-test). **c**, Bioluminescence of lucif-EC grafts with or without MSCs. **d**, Time-dependent quantification of bioluminescence; $^{*}P \le 0.05$, $^{**}P \le 0.01$, $^{***}P \le 0.001$ (n = 3; unpaired t-test). **e**, EC apoptosis assessed by flow cytometry at 24 h post-implantation with/without MSCs, MSC-CM, VEGF, bFGF, and AG1296; $^{*}P \le 0.05$, $^{***}P \le 0.001$ (n = 3; unpaired t-test). **f**, Proteomic dot blotting reveals unique pro-angiogenic factors in MSC-conditioned media. **g**, H&E staining of 7-day explants with multiple conditions; yellow arrowheads indicate perfused vessels. Scale bar, 100 µm. **h**, Day-7 microvessel density; $^{***}P \le 0.001$ (n = 3; unpaired t-test). All data are mean ± s.e.m. *n* are biological replicates (**e**) and independent animals (**b**,**d**,**h**).

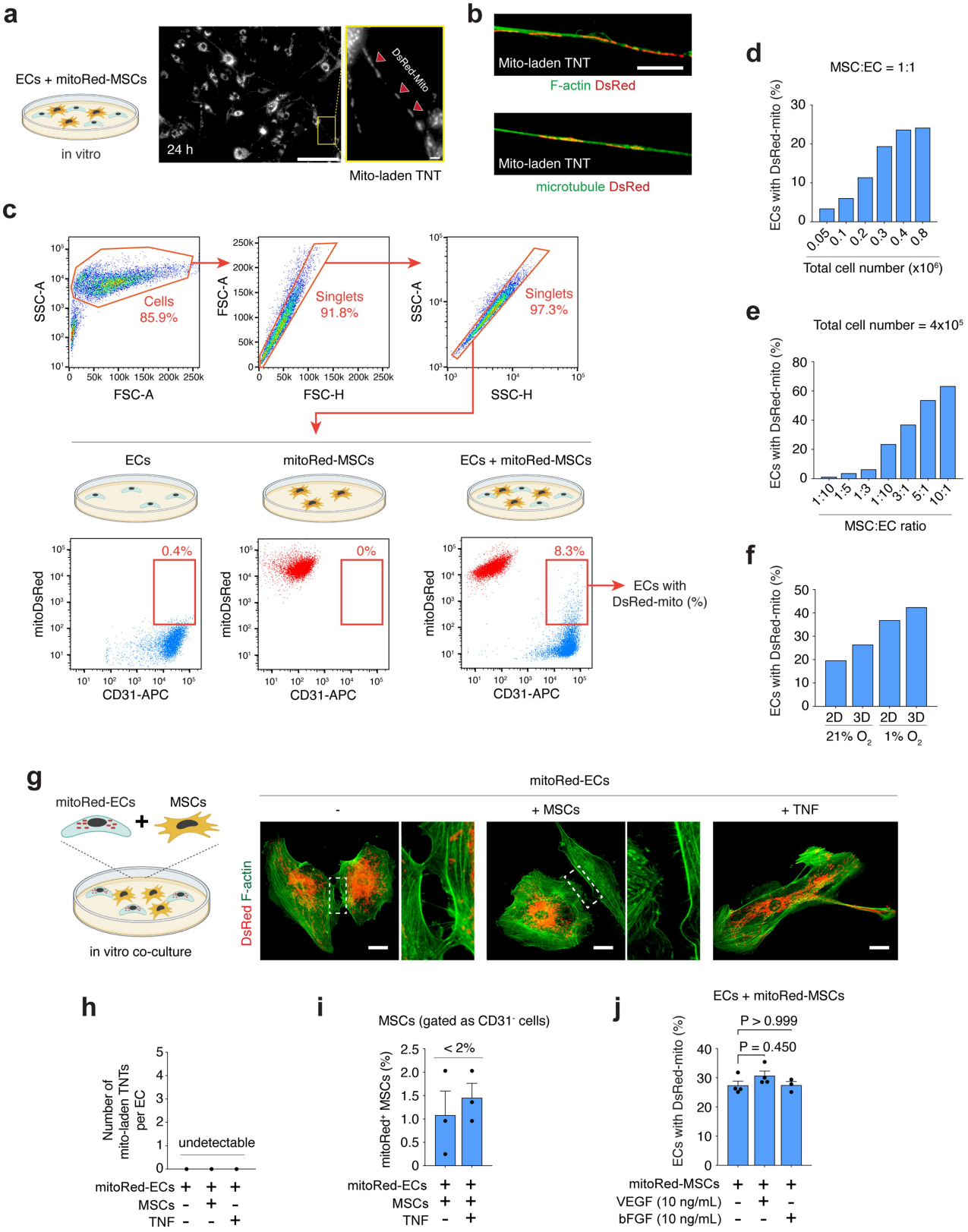

Extended Data Fig. 2 | See next page for caption.

Extended Data Fig. 2 | Formation of mitochondria-laden TNTs by MSCs in the presence of ECs. a, Schematic of 24 h co-culture of mitoRed-MSCs with human ECs. DsRed$^+$ mitochondria in TNTs visualized via fluorescence microscopy. Scale bar, 40 μm. **b**, Immunofluorescence reveals F-actin and microtubule components in TNTs. Scale bar, 5 μm. **c**, Flow cytometry gating strategy to evaluate mitochondrial transfer and eliminate doublets and aggregates. **d**, Proportion of ECs (CD31$^+$) with mitoDsRed$^+$ mitochondria in 1:1 co-culture, indicating plated cell number. **e**, Proportion of mitoDsRed$^+$ mitochondria-receiving ECs at varying MSC:EC ratios, with constant total cell density (4×10^5 cells). **f**, Comparison of mitochondrial transfer in 2D vs. 3D culture and under normoxic vs. hypoxic conditions (4×10^6 cells). **g**, mitoRed-ECs cultured with/without MSCs show negligible DsRed$^+$ mitochondria-laden TNT formation, even after TNF treatment. F-actin visualized by FITC-phalloidin. Scale bars, 10 μm. **h**, Fluorescent quantification confirms minimal TNT formation by ECs under tested conditions (n = 3). **i**, Flow cytometry quantification of DsRed$^+$ mitochondria in MSCs (CD31$^-$) indicates minimal transfer (~1%) from mitoRed-ECs (n = 3). **j**, Proportion of ECs (CD31$^+$) with mitoDsRed$^+$ mitochondria in 1:1 (ECs + mitoRed-MSCs) co-culture in the presence of angiogenic factors VEGF (10 ng/mL) or bFGF (10 ng/mL) (n = 3-4; one-way ANOVA followed by Bonferroni's post-test). All data are mean ± s.e.m. *n* are biological replicates (**h**,**i**,**j**).

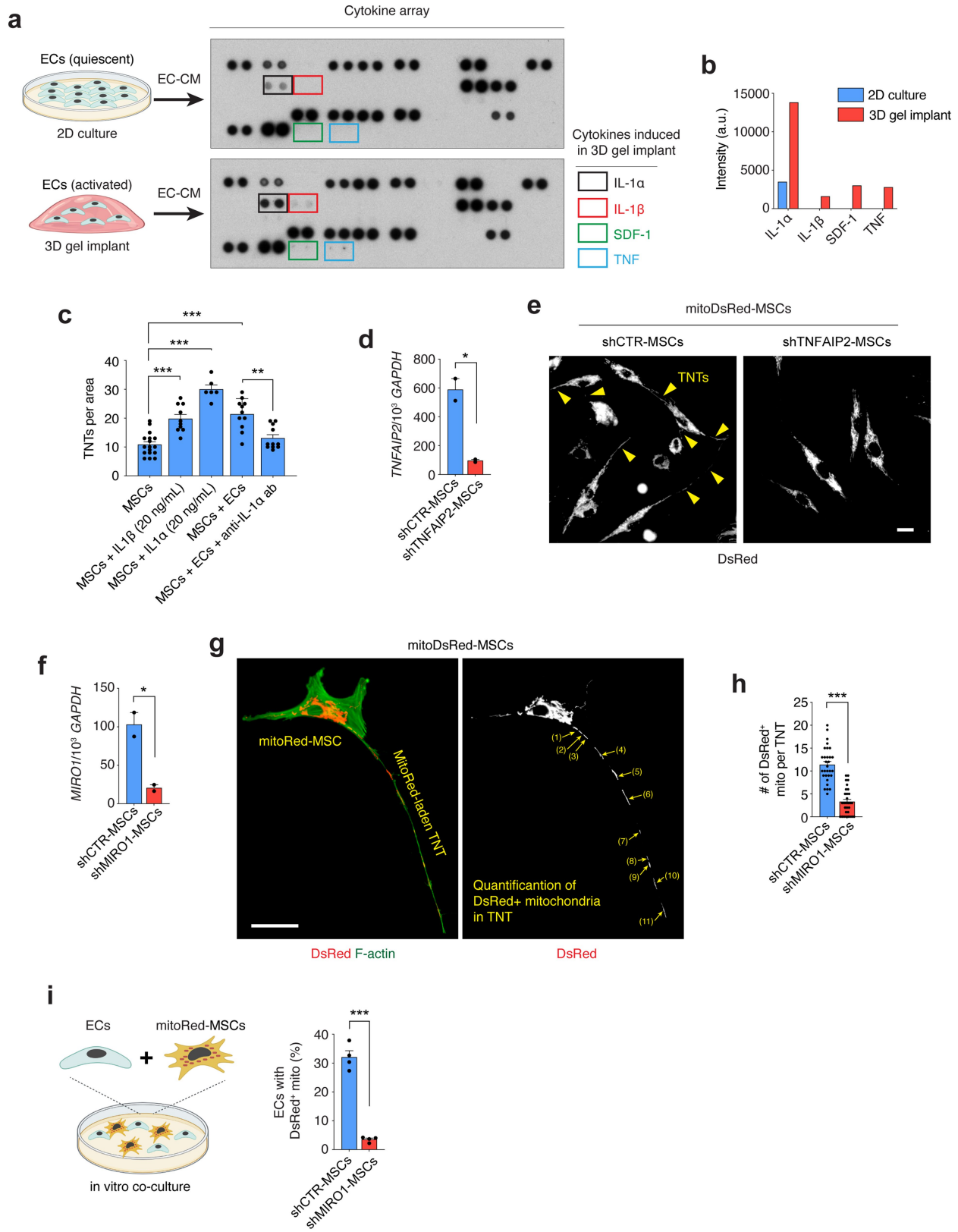

Extended Data Fig. 3 | See next page for caption.

Extended Data Fig. 3 | Regulation of TNT formation and mitochondrial transfer from MSCs to ECs. a, Human ECs cultured in 2D plates or 3D hydrogel had conditioned media analysed for cytokine secretion using proteomic dot blotting arrays; selected cytokines predominantly secreted in 3D are marked. **b**, Blot intensities quantified by ImageJ. **c**, Effect of IL-1α and IL-1β on TNT formation in MSCs. MSCs were exposed to IL-1α, IL-1β, or an anti-IL-1α antibody, and changes in TNT formation were observed and quantified at 24 h. $^{*}P \leq 0.05$, $^{**}P \leq 0.01$, $^{***}P \leq 0.001$ (n = 17, MSCs; n = 10, +IL-1β; n = 6, +IL-1α; n = 11, +ECs; n = 11, +ECs + anti-IL-1α; one-way ANOVA followed by Bonferroni's post-test). **d**, shRNA silencing of TNFAIP2 in mitoRed-MSCs confirmed by qPCR against GAPDH, $^{*}P \leq 0.05$ (n = 2; unpaired two-tailed t-test). **e**, Reduced DsRed^{+} TNTs in shTNFAIP2-MSCs compared to controls; scale bar, 10 μm. **f**, MIRO1 silencing in mitoRed-MSCs confirmed by qPCR, $^{*}P \leq 0.05$ (n = 2; unpaired two-tailed t-test). **g**, F-actin in mitoRed-MSCs visualized by FITC-phalloidin; scale bar, 10 μm. **h**, Lower DsRed^{+} mitochondria count per TNT in shMIRO1-MSCs, $^{***}P \leq 0.001$ (n = 30 TNTs; unpaired two-tailed t-test). **i**, Co-cultures of ECs and mitoRed-MSCs assessed by flow cytometry revealed reduced mitochondrial transfer from shMIRO1-MSCs compared to control MSCs, $^{***}P \leq 0.001$ (n = 4; unpaired two-tailed t-test). All data are mean ± s.e.m. *n* are independent fields (**c**,**h**) and biological replicates (**d**,**f**,**i**,**j**).

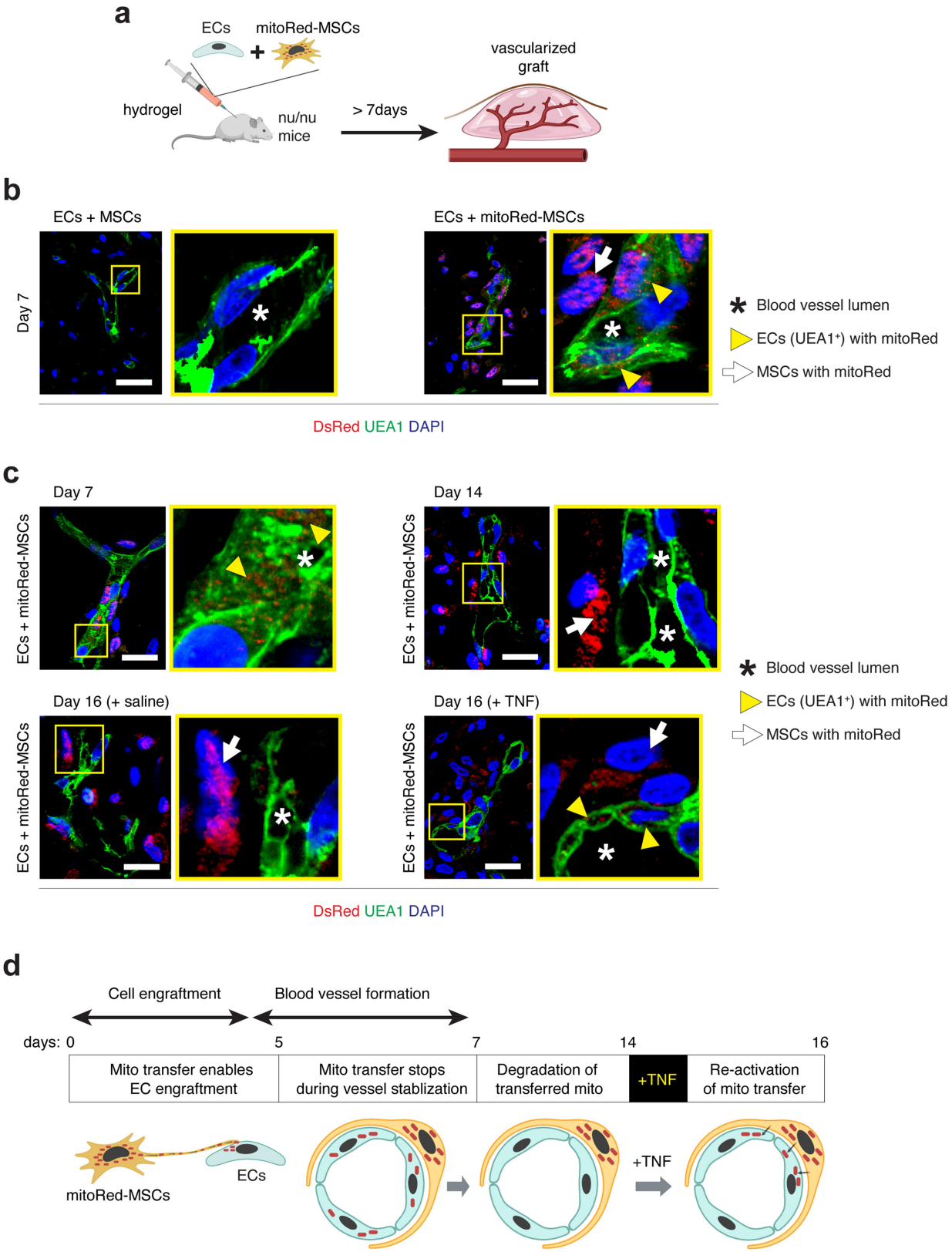

Extended Data Fig. 4 | In vivo temporal dynamics of mitochondrial transfer from MSCs to ECs. a, Depiction of mitoRed-MSCs containing DsRed$^+$ mitochondria and subcutaneously co-transplanted with human ECs into immunodeficient nude mice. **b**, Day-7 post-transplant, immunofluorescence of explanted grafts stained with UEA1 lectin showcases human ECs. Red fluorescence indicates DsRed$^+$ mitochondria, identified with white arrows. UEA1$^+$ ECs containing DsRed$^+$ mitochondria are marked with a yellow arrowhead. Control grafts with unlabelled MSCs, showing no DsRed signal, are displayed on the left. Blood vessel lumens are asterisked. Scale bars, 50 µm. **c**, Different time-point immunofluorescent images of explants highlight DsRed$^+$ mitochondria in UEA1$^+$ ECs (yellow arrowhead) on day 7, absent on day 14. However, administering TNF (contrary to saline) on day 14 reinstated the DsRed$^+$ mitochondrial transfer into UEA1$^+$ ECs, seen on day 16. Scale bars, 50 µm. **d**, Diagram representing the time course appearance of DsRed$^+$ mitochondria (mitoRed) in the grafted ECs.

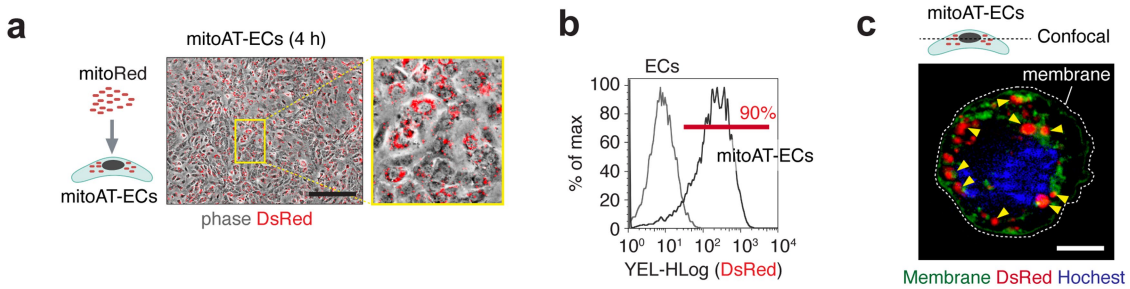

d

pPB-mitoAPEX2 - *piggyBac* vector design

GGAAAGTCT... - APEX2 sequence (678 nucleotides; 225 amino acids)

CTGGCCACC... - Mitochondrial targeting sequence (81 nucleotides; 27 amino acids)

V5 tag - V5 tag (14 amino acids)

attB1 and attB2 - Gateway cloning sites

ATG - Methionine start codon

TAA - Stop codon

pPB-mitoAPEX2 sequence

```
CTCGACGGTATCGATAAGCTATCACAAGTTTGTACAAAAAAGCAGGC
TTAATGCTGGCCACCCGCGTGTTCAGCCTGGTGGGCAAGCGCGCC
ATCAGCACCAGCGTGTGCGTGCGCGCCCACAAGGATCCAGGCAAG
CCCATCCCCAACCCCCTGCTGGGCCTGGACAGCACC
GGAAAGTCTTACCCAACTGTGAGTGCTGATTACCAGGACGCCGTTG
AGAAGGCGAAGAAGAAGCTCAGAGGCTTCATCGCTGAGAAGAGAT
GCGCTCCTCTAATGCTCCGTTTGGCATTCCACTCTGCTGGAACCTTT
GACAAGGGCACGAAGACCGGTGGACCCTTCGGAACCATCAAGCAC
CCTGCCGAACTGGCTCACAGCGCTAACAACGGTCTTGACATCGCTG
TTAGGCTTTTGGAGCCACTCAAGGCGGAGTTCCCTATTTTGAGCTAC
GCCGATTTCTACCAGTTGGCTGGCGTTGTTGCCGTTGAGGTCACGG
GTGGACCTAAGGTTCCATTCCACCCTGGAAGAGAGGACAAGCCTGA
GCCACCACCAGAGGGTCGCTTGCCTGATCCCACTAAGGGTTCTGAC
CATTTGAGAGATGTGTTTGGCAAAGCTATGGGGCTTACTGACCAAGA
TATCGTTGCTCTATCTGGGGGTCACACTATTGGAGCTGCACACAAGG
AGCGTTCTGGATTTGAGGGTCCCTGGACCTCTAATCCTCTTATTTTC
GACAACTCATACTTCACGGAGTTGTTGAGTGGTGAGAAGGAAGGTC
TCCTTCAGCTACCTTCTGACAAGGCTCTTTTGTCTGACCCTGTATTC
CGCCCTCTCGTTGATAAATATGCAGCGGACGAAGATGCCTTCTTTGC
TGATTACGCTGAGGCTCACCAAAAGCTTTCCGAGCTTGGGTTTGCT
GATGCCTAAAACCCAGCTTTCTTGTACAAAGTGGTGATAGCTTGGCG
TAATCATG
```

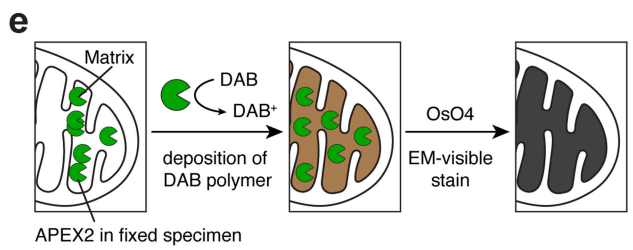

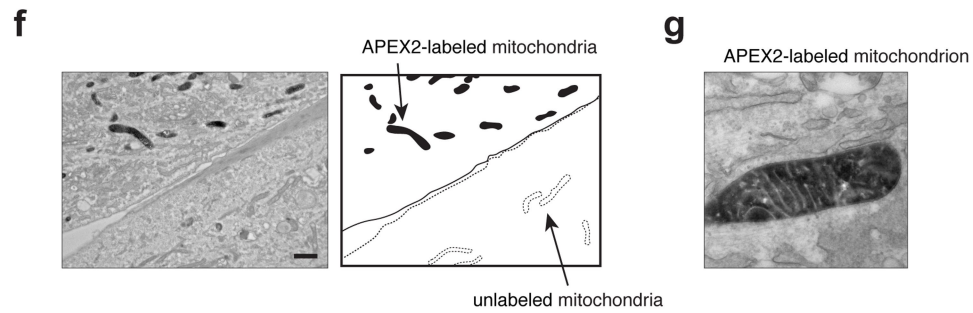

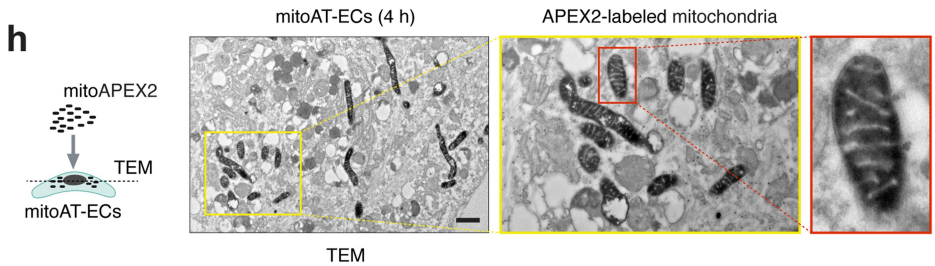

Extended Data Fig. 5 | Artificial transplantation of exogenous mitochondria into human ECs. a, Phase contrast images combined with red fluorescence show cultured ECs 4 h post artificial transplantation with DsRed$^+$ mitochondria (mitoAT-ECs); Scale bar, 200 μm. **b**, Flow cytometry highlights a significant proportion of DsRed$^+$ mitoAT-ECs. **c**, Confocal imaging reveals DsRed$^+$ mitochondria inside mitoAT-ECs; Scale bar, 10 μm. **d**, Depiction of the pPB-mitoAPEX2 piggyBac vector carrying APEX2 and mitochondria-targeting sequences. APEX2, an enhanced soybean ascorbate peroxidase, acts as a tag for TEM. **e**, Method to visualize APEX2$^+$ mitochondria using TEM: APEX2-expressing cells are fixed, then treated with diaminobenzidine (DAB) and hydrogen peroxide. APEX2 catalyses the DAB polymerization, generating TEM contrast after osmium treatment. **f**, TEM contrasts APEX2-labelled mitochondria in mitoAPEX2-transfected cells with unlabelled counterparts in controls; Scale bar, 500 nm. **g**, High-magnification TEM of an APEX2-labelled mitochondrion. **h**, Mitochondria from mitoAPEX2-MSCs transplanted into ECs show APEX2$^+$ mitochondria in mitoAT-ECs at 4 h; Scale bar, 500 nm.

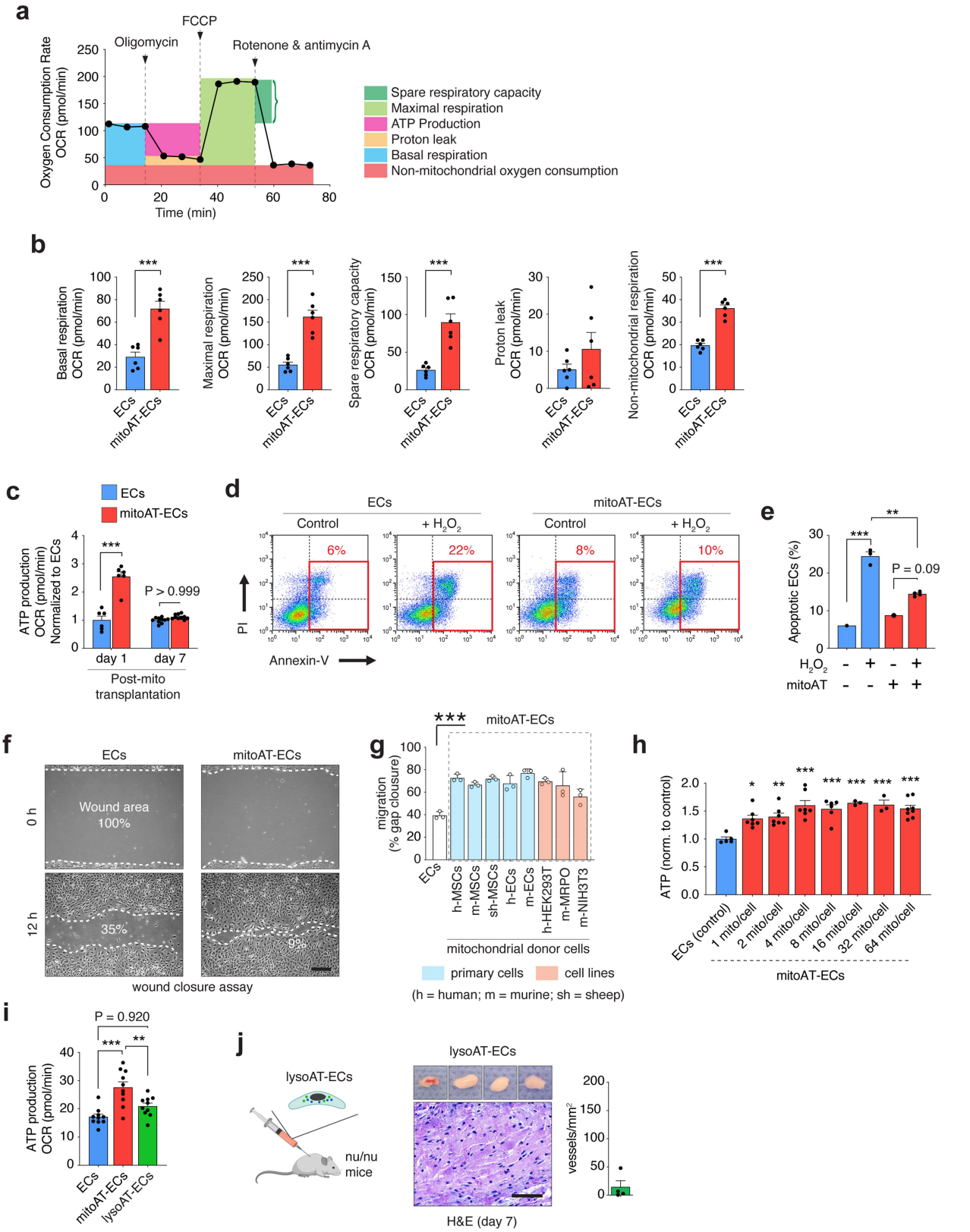

Extended Data Fig. 6 | See next page for caption.

Extended Data Fig. 6 | Enhanced mitochondrial respiration, apoptosis resistance and migration capacity in mitoAT-ECs. a, Schematic of OCR profile (Seahorse analysis) with specific mitochondrial respiration parameters. Abbreviations: FCCP, carbonyl cyanide-p-trifluoromethoxyphenyl hydrazone. **b**, Basal respiration, maximal respiration, spare respiratory capacity, proton leak, and non-mitochondrial respiration in ECs and mitoAT-ECs. ***P ≤ 0.001 (n = 6; unpaired two-tailed t-test). **c**, ATP production in mitoAT-ECs measured at 1 and 7 days after a one-time artificial mitochondrial transplantation. ***P ≤ 0.001 (n = 6 at day 1, n = 10 at day 7; unpaired two-tailed t-test). **d**, Post-mitochondrial transplantation, mitoAT-ECs exposed to 200 µM H_2O_2 for 12 h were analysed for apoptosis using flow cytometry (PI/Annexin-V staining), with non-transplanted ECs as controls. **e**, Percentage of apoptotic (Annexin-V^+) ECs post H_2O_2 exposure. **P ≤ 0.01, ***P ≤ 0.001 (n = 3-4; one-way ANOVA with Bonferroni's post-test). **f**, A standard wound closure assay depicts migration capacity, with wound areas at 0 h and 12 h in mitoAT-ECs compared to control ECs. **g**, Quantification of wound gap closure in mitoAT-ECs transplanted with mitochondria from various donors, indicating improved closure rates, ***P ≤ 0.001 (n = 3; one-way ANOVA followed by Bonferroni's post-test). **h**, Relative ATP production levels in ECs measured 24 h after receiving different concentrations of mitochondria (mitoAT-ECs). ECs without mitochondrial transfer served as control. *P ≤ 0.05, **P ≤ 0.01, ***P ≤ 0.001 compared to control (n = 3–7; unpaired two-tailed t-test). **i**, Comparison of ATP production in ECs transplanted with exogenous mitochondria (mitoAT-ECs) or lysosomes (lysoAT-ECs). **P ≤ 0.01, ***P ≤ 0.001 (n = 10; one-way ANOVA with Bonferroni's post-test). **j**, Histological evaluations of subcutaneous grafts with lysoAT-ECs at 7 days post-transplantation. Scale bar, 100 µm. Quantitative analysis of microvascular density displaying reduced vascularization potential (n = 4). All data are mean ± s.e.m. *n* are biological replicates (**b**,**c**,**e**,**g**,**h**,**i**) and independent animals (**j**).

a

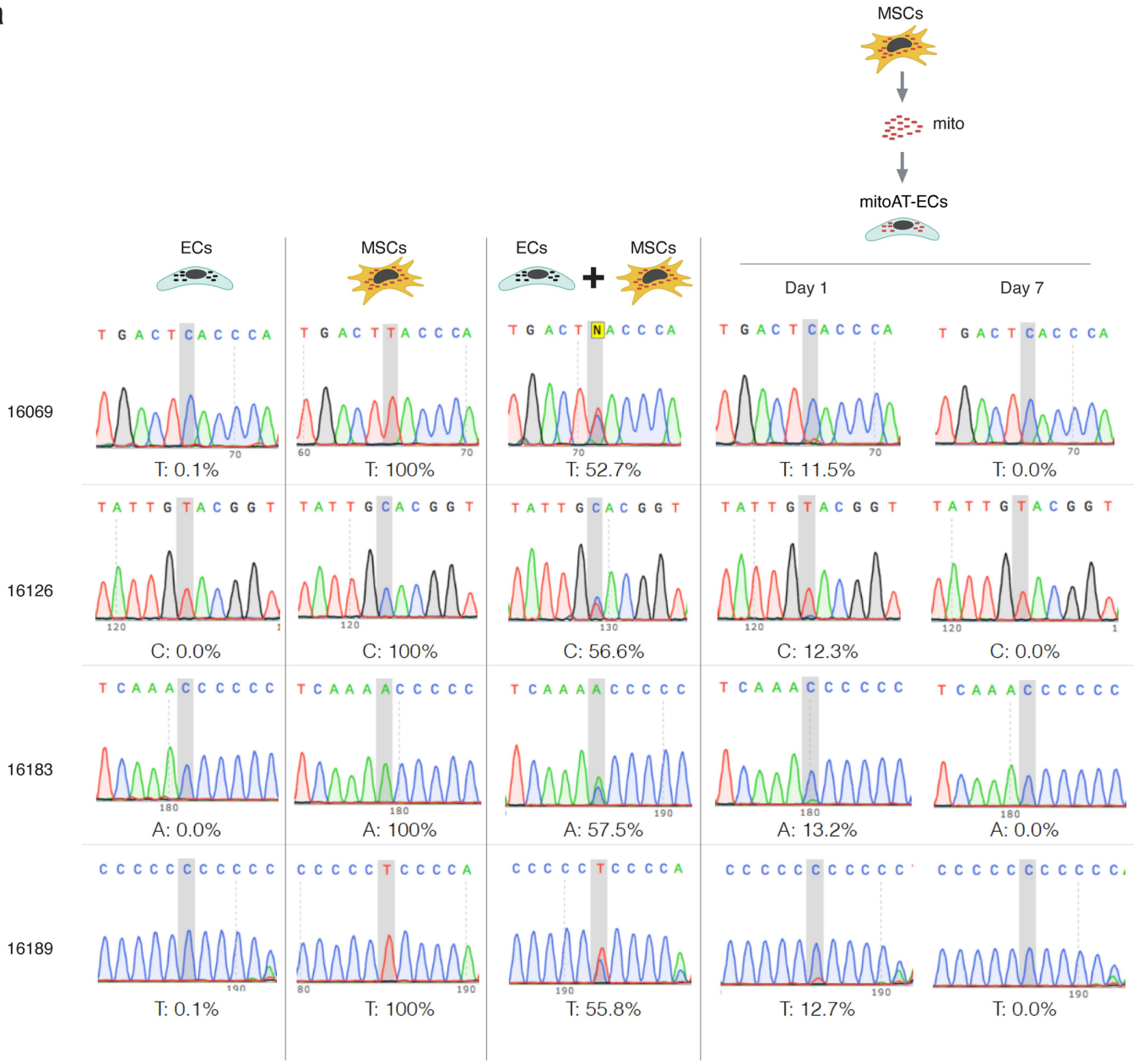

b

locus	ECs	MSCs
16069	TGACTCACCCA	TGACTTACCCA
16126	TATTGTACGGT	TATTGCACGGT
16183	TCAAACCCCCC	TCAAAACCCCC
16189	CCCCCCCCCCC	CCCCCTCCCCC

mtDNA heteroplasmy

Extended Data Fig. 7 | Temporal analysis of mtDNA heteroplasmy in mitoAT-ECs after mitochondrial transplantation. a, mtDNA sequencing showcases four specific loci with heteroplasmy in hypervariable regions, highlighting a single nucleotide difference between ECs and MSCs. Depicted sequences represent ECs (monoculture), MSCs (monoculture), ECs + MSCs (1:1 co-culture), and mitoAT-ECs (monoculture) for the chosen loci. **b**, Summary table detailing heteroplasmy at four loci in the hypervariable mtDNA regions across ECs and MSCs.

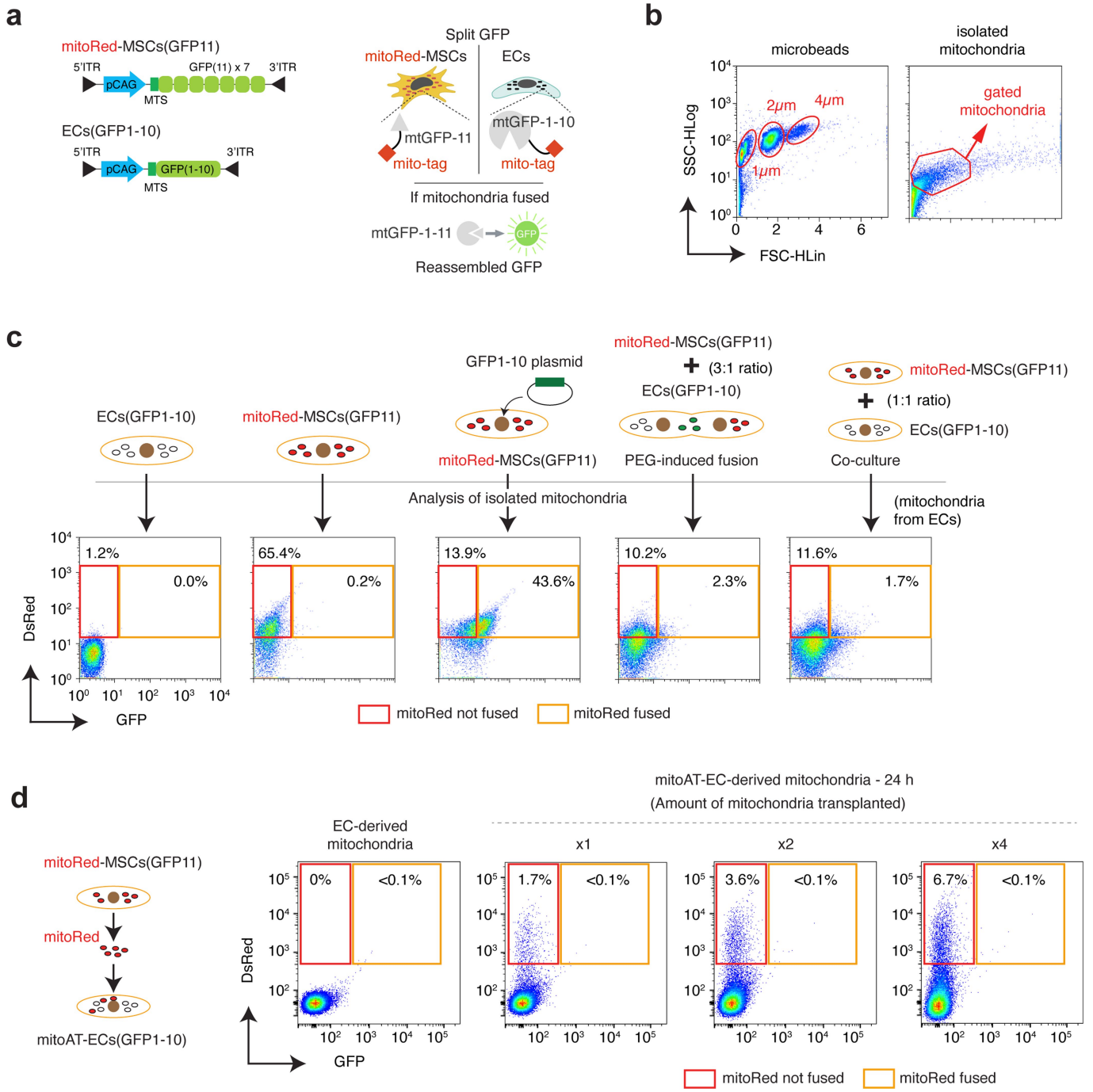

Extended Data Fig. 8 | Quantitative flow cytometry analysis of exogenous mitochondrial integration using the split-GFP system. a, Schematic of the split-GFP system, with GFP-1–10 in EC mitochondria and GFP-11 in mitoRed-MSCs. Fluorescence signals fusion between MSC-derived and EC mitochondria. **b**, Flow cytometry gating strategy for mitochondria, using size-specific microbeads as reference. **c**, Flow cytometry analysis of isolated mitochondria illustrating the proportion of non-fused DsRed$^+$ (red box) and fused DsRed$^+$GFP$^+$ (yellow box) mitochondria across experimental groups. **d**, Mitochondrial integration post-transplantation analysis. Proportions of DsRed$^+$ (red box) and DsRed$^+$GFP$^+$ (yellow box) in mitoAT-EC-derived mitochondria assessed at 24 h post-transplantation, with EC-derived mitochondria as the negative control. Representative flow cytometry data showing a dose-dependent increase in DsRed+ mitochondria at 24 h with double (×2) and quadruple (×4) transplanted mitochondria, consistently <0.1% GFP$^+$.

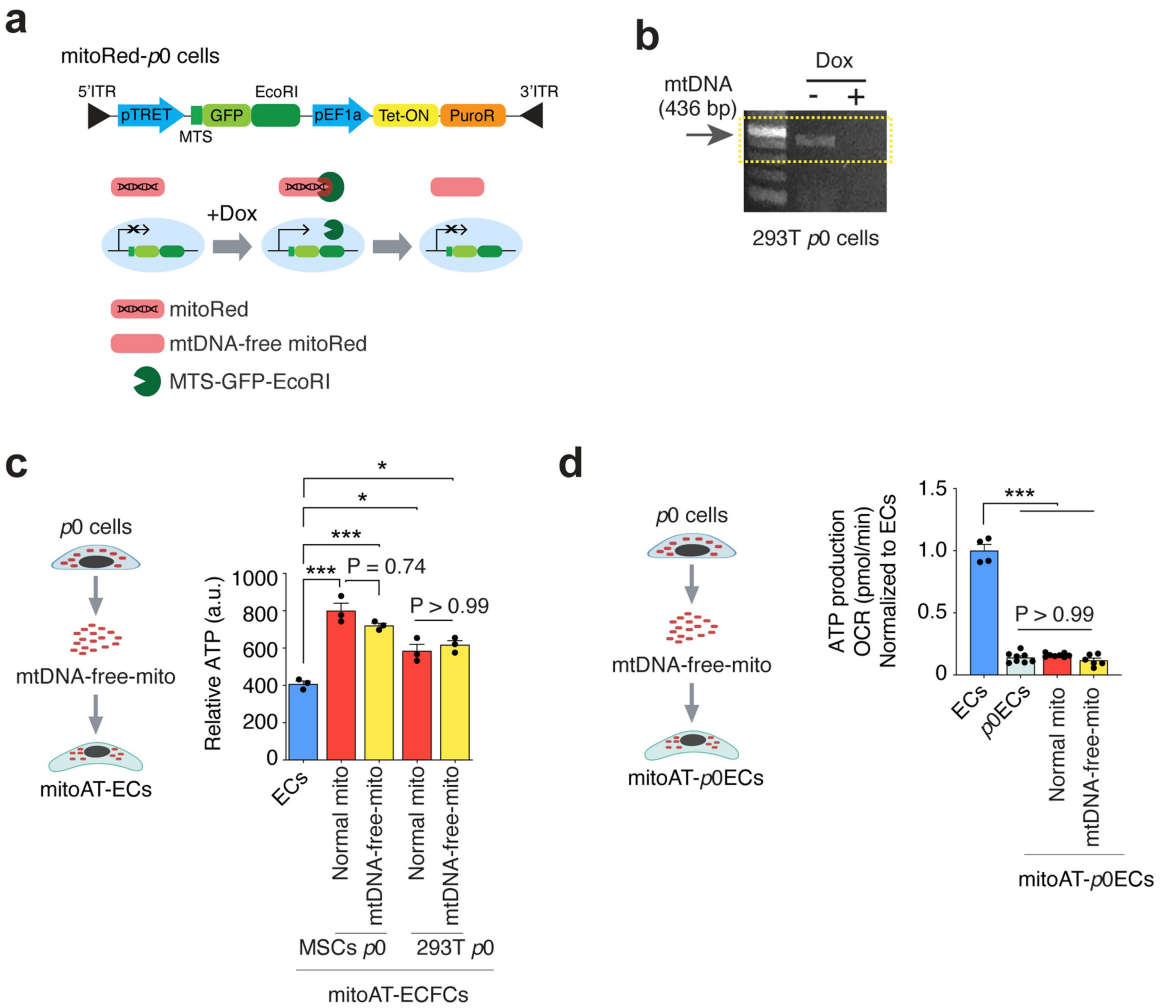

Extended Data Fig. 9 | Transplantation of mtDNA-free mitochondria enhances ATP in ECs. a, Diagram illustrating the engineering of mtDNA-free cells (mitoRed-ρ0) using a Dox-regulated MTS-EcoRI-GFP complex for mtDNA degradation. **b**, PCR gel confirms the thorough depletion of mtDNA in the mitoRed-ρ0-293T cell line after a 48-hour Dox treatment. **c**, Transplantation of mtDNA-free mitochondria from mitoRed-ρ0-MSCs into ECs. Quantification of ATP production in both ECs and mitoAT-ECs. *P ≤ 0.05, ***P ≤ 0.001 (n = 3; one-way ANOVA with Bonferroni's post-test). **d**, Transplantation of normal and mtDNA-free mitochondria into ρ0-ECs. ATP production in ρ0-ECs measured before and 24 h after exogenous mitochondrial transplantation. ***P ≤ 0.001 (n = 4, ECs; n = 8, ρ0-ECs; n = 8, mitoAT-ECs with normal mito; n = 6, mitoAT-ECs with mtDNA-free mito; one-way ANOVA followed by Bonferroni's post-test). All data are mean ± s.e.m. *n* are biological replicates (**c**,**d**).

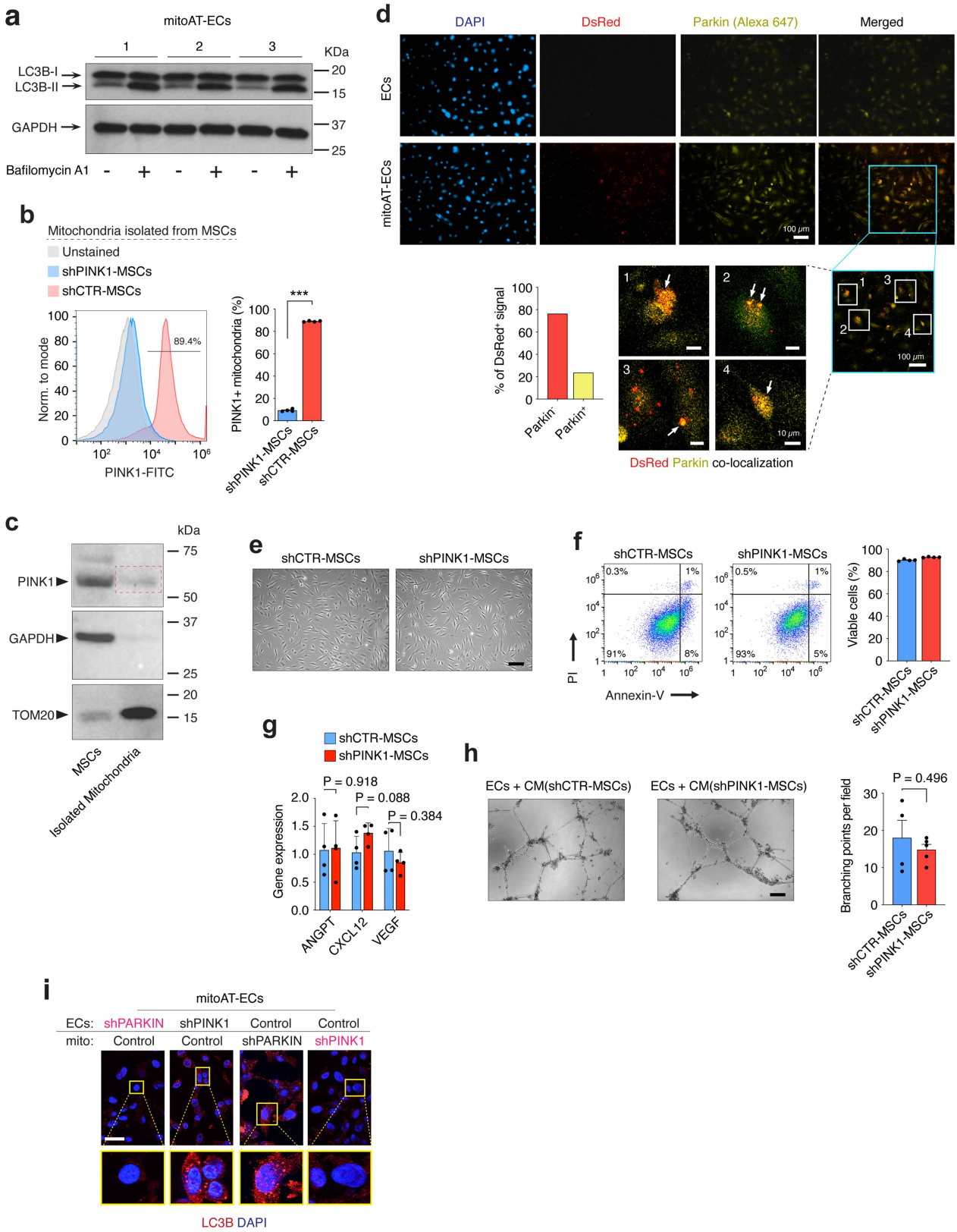

Extended Data Fig. 10 | See next page for caption.

Extended Data Fig. 10 | Exogenous mitochondrial transplantation induces mitophagy in mitoAT-ECs. a, Analysis of autophagic flux in mitoAT-ECs, showing LC3B-I to LC3B-II conversion with Bafilomycin A1. **b**, Flow cytometry analysis showing PINK1 presence on isolated mitochondria from control MSCs (shCTR-MSCs) but not from shPINK1-MSCs. Quantification of the percentage of PINK1-positive in isolated mitochondria from control versus shPINK1-MSCs. ***P ≤ 0.001 (n = 4; unpaired two-tailed t-test). **c**, Western blot analysis demonstrating the presence of PINK1 (63 kDa) in lysates from both MSCs and isolated mitochondria (red line box), with TOM20 (16 kDa) as a mitochondrial marker and GAPDH (36 kDa) as a cytosolic control. **d**, Immunofluorescence indicates co-localization of exogenous DsRed+ mitochondria (Red) with endogenous Parkin (Alexa 647) in mitoAT-ECs 24 h post-transplantation (white arrows). Scale bar, 100 µm; insets #1–4, 10 µm. **e**–**h**, Evaluation of MSC viability and functionality after PINK1 silencing (shRNA). **e**, Morphological observations of MSCs with shRNA against PINK1 (shPINK1-MSCs) vs. control shRNA (shCTR-MSCs) show standard mesenchymal cell morphology. Scale bar, 100 µm. **f**, Flow cytometry using PI/Annexin-V highlights the high viability of shPINK1-MSCs after lentiviral transduction (n = 4). **g**, qPCR analysis measures angiogenic growth factor expression (ANGPT, CXCL12, VEGF) in shCTR-MSCs vs. shPINK1-MSCs (n = 4; unpaired two-tailed t-test). **h**, In vitro assay of EC vascular network formation, using conditioned medium (CM) from shPINK1-MSCs vs. shCTR-MSCs (n = 4; unpaired two-tailed t-test). Scale bar, 200 µm. **i**, Immunofluorescence detection of LC3B+ autophagosomes in mitoAT-ECs. Effects of Parkin and PINK1 silencing (shRNA) in either the donor MSC mitochondria (mito) or recipient ECs. DAPI denotes cell nuclei. Scale bar, 10 µm. All data are mean ± s.e.m. *n* are biological replicates (**b**,**f**,**g**,**h**). For gel source data, see Supplementary Fig. 1.

nature portfolio

Corresponding author(s): Juan Melero-Martin

Last updated by author(s): Feb 15, 2024

Reporting Summary

Nature Portfolio wishes to improve the reproducibility of the work that we publish. This form provides structure for consistency and transparency in reporting. For further information on Nature Portfolio policies, see our Editorial Policies and the Editorial Policy Checklist.

Statistics

For all statistical analyses, confirm that the following items are present in the figure legend, table legend, main text, or Methods section.

n/a	Confirmed
☐	☒ The exact sample size (*n*) for each experimental group/condition, given as a discrete number and unit of measurement
☐	☒ A statement on whether measurements were taken from distinct samples or whether the same sample was measured repeatedly
☐	☒ The statistical test(s) used AND whether they are one- or two-sided *Only common tests should be described solely by name; describe more complex techniques in the Methods section.*
☐	☒ A description of all covariates tested
☐	☒ A description of any assumptions or corrections, such as tests of normality and adjustment for multiple comparisons
☐	☒ A full description of the statistical parameters including central tendency (e.g. means) or other basic estimates (e.g. regression coefficient) AND variation (e.g. standard deviation) or associated estimates of uncertainty (e.g. confidence intervals)
☐	☒ For null hypothesis testing, the test statistic (e.g. *F*, *t*, *r*) with confidence intervals, effect sizes, degrees of freedom and *P* value noted *Give P values as exact values whenever suitable.*
☒	☐ For Bayesian analysis, information on the choice of priors and Markov chain Monte Carlo settings
☒	☐ For hierarchical and complex designs, identification of the appropriate level for tests and full reporting of outcomes
☒	☐ Estimates of effect sizes (e.g. Cohen's *d*, Pearson's *r*), indicating how they were calculated

Our web collection on statistics for biologists contains articles on many of the points above.

Software and code

Policy information about availability of computer code

Data collection	Information provided in the Method section. Instruments included: IVIS 200 Imaging System - Xenogen Corporation FACSAria II 5-LASER sorter system - BD Biosciences BD FACS LSRFortessa - BD Biosciences Z1 inverted microscope - Carl Zeiss AxioCam MRc5 camera - Carl Zeiss G:Box Chemi XX6/XX9 - Syngene Microplate Reader and Cell counting - Spark™ - Tecan
Data analysis	Data analysis software: Live Image 3.0 - Xenogen Corporation ImageJ 1.52a - Open Source Seahorse XFe96 Analyzer - Agilent R package ClusterProfiler v 4.6.2 - Open Source AxioVision Rel. 4.8 software - Carl Zeiss GraphPad Prism v 9 - GraphPad FlowJo software v 10.62 - Tree Star Inc GeneSys control software - Syngene

For manuscripts utilizing custom algorithms or software that are central to the research but not yet described in published literature, software must be made available to editors and reviewers. We strongly encourage code deposition in a community repository (e.g. GitHub). See the Nature Portfolio guidelines for submitting code & software for further information.

Data

Policy information about availability of data

All manuscripts must include a data availability statement. This statement should provide the following information, where applicable:

- Accession codes, unique identifiers, or web links for publicly available datasets
- A description of any restrictions on data availability
- For clinical datasets or third party data, please ensure that the statement adheres to our policy

The authors declare that all data supporting the findings of this study are available in the paper and its Supplementary Information.
For RNAseq analysis, reads were then aligned to UCSC (University of California, Santa Cruz) hg38 genome (STAR aligner). Reference genome (hg38.fa.gz) and genome annotation file (hg38.knownGene.gtf.gz) are both publicly available from UCSC Genome Browser (https://genome.ucsc.edu/cgi-bin/hgGateway).

Human research participants

Policy information about studies involving human research participants and Sex and Gender in Research.

Reporting on sex and gender	Not applicable
Population characteristics	Not applicable
Recruitment	Not applicable
Ethics oversight	Not applicable

Note that full information on the approval of the study protocol must also be provided in the manuscript.

Field-specific reporting

Please select the one below that is the best fit for your research. If you are not sure, read the appropriate sections before making your selection.

☒ Life sciences ☐ Behavioural & social sciences ☐ Ecological, evolutionary & environmental sciences

For a reference copy of the document with all sections, see nature.com/documents/nr-reporting-summary-flat.pdf

Life sciences study design

All studies must disclose on these points even when the disclosure is negative.

Sample size	Samples size, including number of mice per group, were determined to ensure adequate power and were based on the means and variations observed in our pilot experiments our and historical data.
Data exclusions	No data were excluded. No exclusion criteria were applied for all analyses.
Replication	All experiments were independently replicated at least three times.
Randomization	Mice were randomly selected and allocated groups for each type of experiment.
Blinding	The study involved unbiased quantification and analysis for bioluminescence, immunostaining, and gene expression data sets. There was no expected outcome prior to the analysis, and blinding is not relevant.

Reporting for specific materials, systems and methods

We require information from authors about some types of materials, experimental systems and methods used in many studies. Here, indicate whether each material, system or method listed is relevant to your study. If you are not sure if a list item applies to your research, read the appropriate section before selecting a response.

Materials & experimental systems

n/a	Involved in the study
☐	☒ Antibodies
☒	☐ Eukaryotic cell lines
☒	☐ Palaeontology and archaeology
☐	☒ Animals and other organisms
☒	☐ Clinical data
☒	☐ Dual use research of concern

Methods

n/a	Involved in the study
☒	☐ ChIP-seq
☐	☒ Flow cytometry
☒	☐ MRI-based neuroimaging

Antibodies

Antibodies used

α-SMA Monoclonal (Clone: 1A4), 1:1000, Sigma, Catalog #A2547, PMID: [28868207]
β-Actin (Clone: ARC5115-01), 1:20000, Abclonal, Catalog #AC038, PMID: [37095076]
β-Actin Monoclonal, 1:10000, Abcam, Catalog #8226, PMID: [26984724]
CD31 Monoclonal (Clone: WM59), 1:1000, BD Biosciences, Catalog #555445, PMID: [24982174]
CD31 Monoclonal (Clone: JC70A), 1:1000, Agilent, Catalog #M082329-2, PMID: [24982174]
CD90 (Clone: 5E10), 1:1000, eBioscience, Catalog #17-0909-41, PMID: [24982174]
GAPDH Polyclonal, 1:5000, Sigma, Catalog #G9545, PMID: [37739965]
IL-1α Monoclonal (Clone: A15032A), 1:1000, Biolegend, Catalog #686502, PMID: [32979835]
LC3B Polyclonal, 1:1000, Abcam, Catalog #ab51520, PMID: [32312955]
LC3B Polyclonal, 1:1000, Cell Signaling, Catalog #2775, PMID: [23205553]
Parkin Monoclonal (Clone: PRK8), 1:2000, Abcam, Catalog #ab77924, PMID: [32312955]
PINK1 Polyclonal, 1:1000, NOVUS Biological Inc, Catalog #BC100-494, PMID: [28683321], [24189060]
PINK1 Polyclonal, 1:1000, Thermo Fisher, Catalog #PA5-86941, PMID: [37152664]
TOM20 Monoclonal, 1:1000, Abcam, Catalog #ab56783, PMID: [37537168], [31952989]
Tubulin Monoclonal (Clone: EP1332Y), 1:1000, Abcam, Catalog #ab52866, PMID: [29362447]
TNFα Neutralizing Rabbit Monoclonal (Clone: D1B4), 10 ng/mL, Cell Signaling, Catalog #7321S, PMID: [27314284]

Validation

Antibodies were previously validated in the references stated above (PMID).

Animals and other research organisms

Policy information about studies involving animals; ARRIVE guidelines recommended for reporting animal research, and Sex and Gender in Research

Laboratory animals	Mice. Athymic nude mice, 6-9 weeks of age, male. Mice were housed under a 12-hour dark/light cycle with ambient temperature maintained at 68-74 degrees F and relative humidity at 30-70%.
Wild animals	The study did not involve wild animals.
Reporting on sex	Sex was not considered as a variable in this study due to the use of male nude mice only.
Field-collected samples	The study did not involve field-collected samples.
Ethics oversight	All animal-related protocols were approved by the Institutional Animal Care and Use Committee at Boston Children's Hospital.

Note that full information on the approval of the study protocol must also be provided in the manuscript.

Flow Cytometry

Plots

Confirm that:

☒ The axis labels state the marker and fluorochrome used (e.g. CD4-FITC).

☒ The axis scales are clearly visible. Include numbers along axes only for bottom left plot of group (a 'group' is an analysis of identical markers).

☒ All plots are contour plots with outliers or pseudocolor plots.

☒ A numerical value for number of cells or percentage (with statistics) is provided.

Methodology

Sample preparation

Cells were dissociated into single-cell suspensions using TryPLE and washed with PBS supplemented with 1% BSA and 0.2 mM EDTA.

Instrument	Guava easyCyte 6HT/2L flow cytometer (Millipore Corporation, Billerica, MA) and BD Accuri C6 Flow Cytometer, BD FACS LSRFortessa, and BD FACSAria™ II Cell Sorter (BD Biosciences, San Jose, CA).
Software	FlowJo software (Tree Star Inc., Ashland, OR)
Cell population abundance	Cell population abundance is consistently reported throughout the Result section of the manuscript.
Gating strategy	Routine preliminary FSC/SSC gating conducted throughout. Any other gating strategy based on fluorescent signals are consistently reported throughout the Result section of the manuscript.

☒ Tick this box to confirm that a figure exemplifying the gating strategy is provided in the Supplementary Information.